Flat band induced topological photonic Tamm states in stubbed structures: Theory and experiment

Soufyane Khattou, Yamina Rezzouk, Mohamed El Ghafiani, Madiha Amrani, Mohammed Elaouni, El Houssaine El Boudouti, Abdelkrim Talbi, Abdellatif Akjouj, Bahram Djafari-Rouhani

Flat band induced topological photonic Tamm states in stubbed structures: Theory and experiment

Soufyane Khattou,[1] Yamina Rezzouk,[1] Mohamed El Ghafiani,[1] Madiha Amrani,[1] Mohammed Elaouni,[1] El Houssaine El Boudouti,[1,*] Abdelkrim Talbi,[2] Abdellatif Akjouj,[3] and Bahram Djafari-Rouhani[3]

[1]*LPMR, Département de Physique, Faculté des Sciences, Université Mohammed I, Oujda, Morocco*

[2]*Université de Lille, CNRS, Centrale Lille, ISEN, Université de Valenciennes, UMR 8520, IEMN, LIA LICS/LEMAC, F-59000 Lille, France*

[3]*IEMN, UMR CNRS 8520, Département de Physique, Université de Lille, 59655 Villeneuve d'Ascq, France*

(Received 30 December 2022; accepted 21 February 2023; published 7 March 2023)

We provide theoretical and experimental evidence for the existence of topological Tamm states at the interface between two stubbed photonic crystals (PCs) as a function of the period and length of the stubs. Several works have addressed these states in the well-known Su-Schrieffer-Heeger model, a dimerized chain based on two resonators per unit cell where the opening of a gap at a Dirac cone results in a symmetry inversion of bulk bands between two topologically different crystals. Here, we give a detailed theoretical analysis of a mechanism based on band-edge symmetry inversion around a flat band, i.e., when the width of the pass band vanishes, while using only one resonator (stub) per unit cell. Then, we propose a simple versatile experimental platform to observe such interface states, which is based on coaxial cables operating in the radio-frequency domain. The investigation of these states was performed by using different approaches: (i) the topology of the bands based on the Zak phase and the symmetry of the band-edge modes, (ii) the sign of the reflection phase between each PC and a waveguide, and (iii) the dips or peaks in the reflection and transmission spectra when two finite photonic crystals are connected together either horizontally or vertically along a waveguide. Furthermore, we give a general rule about the existence of interface states when two PCs exhibit two common gaps with a flat band in their middle and different bulk-edge symmetries. Also, we provide closed-form expressions of the geometrical parameters and the frequency for which the interface state becomes bound state in the continuum (BIC). We show that these topological BIC states are stationary states of the cavity between the two PCs, and are very robust to any perturbation on both sides of the cavity. Finally, we show the impossibility of existence of interface states between two PCs with identical periods and different stubs. The theoretical and experimental results are discussed for both Neumann and Dirichlet boundary conditions at the end of the stubs.

DOI: 10.1103/PhysRevB.107.125405

I. INTRODUCTION

Tamm states are electronic surface states localized at the surface termination of a crystal due to the periodicity breaking [1,2]. They appear as defect eigenmodes in the gaps of the crystal [3]. Surface states can appear also at the boundaries of periodic photonic crystals (PCs), due to the similar wave nature of electrons and photons [4–7]. These modes are called optical Tamm states [8,9]. Surface modes in one-dimensional (1D) dielectric Bragg mirrors or superlattices in contact with vacuum or other homogeneous materials have been extensively studied theoretically [4–8,10–12] and experimentally [9,13–18]. In addition to dielectric-dielectric multilayers, surface waves in other types of periodic structures have been investigated such as dielectric-plasma [19,20], dielectric-graphene [21,22], metamaterials [23,24], plasmonic waveguides [25,26] and photonic circuits [27–29]. In addition to surface states in one PC, several works have addressed interface states between two different PCs with overlapping gaps [30–32]. Surface and interface states in PCs have been proposed for different applications such as sensors [33,34], reduced light absorption [35,36], and polariton lasers [30,36].

Recently, considerable efforts have been dedicated to the search of interface states between a PC and a homogeneous material or between two PCs based on the concept of topological invariant and the geometric phases of the bulk bands [37–51]. In 1D periodic materials, the topology of the bands is determined via the calculation of the Zak phase [52], which is a kind of Berry phase spanning the first Brillouin zone [53]. Experimentally, the Zak phase of the bands as well as the topological interface states between two PCs are determined from the reflection phase [40,41] and transmission and reflection amplitude [48,49], respectively. There exists numerous models that enable to describe the existence of topological interface states between two PCs [54]. One of the most popular models is the Su-Schieffer-Heeger (SSH) model [55] based on the concept of band inversion (gapless). In this model, the interface mode is obtained by connecting two PCs with inverted symmetry of their bulk-edge modes on both sides of a gap opened at a Dirac point [48,49,51]. These modes are characterized by their robustness to perturbation and disorder

*Corresponding author: elboudouti@yahoo.fr

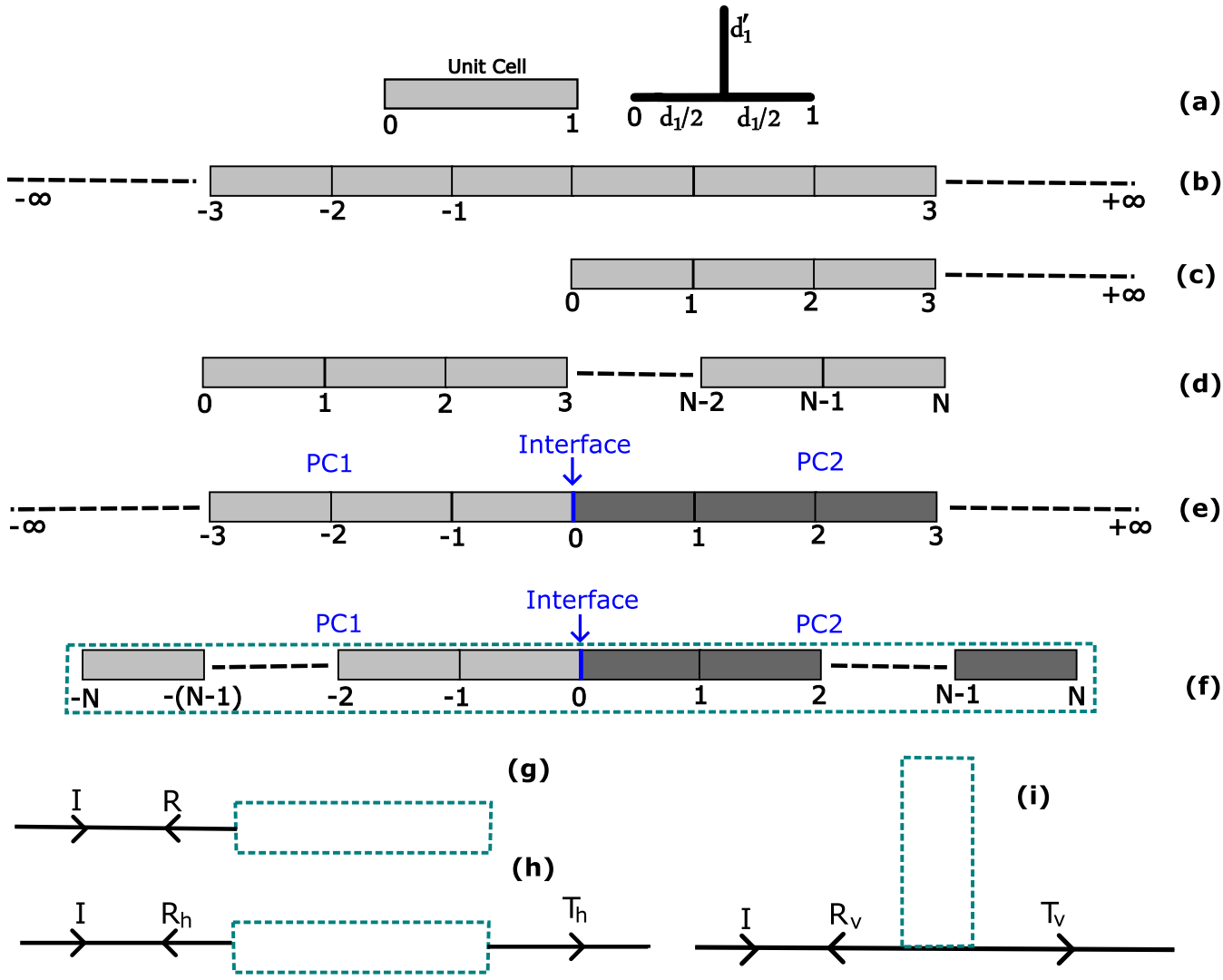

FIG. 1. (a) Symmetric unit cell in the space of interfaces {0, 1}. In the following sections, the unit cell is made of a stub of length d_1' inserted in the middle of a segment of length d_1. (b) Infinite PC made of periodic symmetric cells. (c) Semi-infinite PC made of periodic symmetric cells. (d) Finite PC made of N periodic symmetric cells. (e) Interface between two semi-infinite PCs. (f) Interface between two finite PCs. (g) Two PCs as in (f) attached to one semi-infinite waveguide. (h) Two PCs as in (f) inserted between two semi-infinite waveguides. (i) Two PCs as in (f) grafted vertically along a waveguide.

in the system [48,49]. The SSH model has also been used to predict the existence of surface modes in just one PC in contact with air or another dielectric [50]. Let us mention that for some geometrical parameters, the interface state can become a bound state in the continuum (BIC) which is characterized by an infinite lifetime (i.e., infinite quality factor) [56]. Some recent works have addressed topological BIC in photonic crystals based on dielectric arrays and photonic slabs [57–61].

In the SSH model, dimerized systems with two similar resonators in a unit cell provide another degree of freedom compared to the simple lattice, resulting in the nontrivial topological phase and edge states. The edge states appear as a consequence of gap closing and reopening. Recently, stubbed waveguides have been treated by considering two stubs by unit cell in the framework of SSH model [51]. Here, we provide another mechanism that enables to predict the existence of edge states between two PCs which is based on band closing (or flat bands). This phenomenon occurs around flat bands where the gaps are of hybridization type instead of being Bragg type. First, we give a general theory that enables to study the interface states between any two PCs made of symmetric cells. In this theory, we provide the dispersion relation and local density of the states (LDOS) between two semi-infinite PCs as well as the transmission and reflection coefficients and total DOS of two connected finite PCs. Then, we give an application of this theory to a comb structure made of stubs of length d_1' grafted in the middle of a segment of length d_1 (Fig. 1). The boundary conditions at the end of the stubs can be either Neumann boundary condition (NBC) [i.e., vanishing of the magnetic field ($H = 0$)] or Dirichlet boundary condition (DBC) [i.e., vanishing of the electric field ($E = 0$)]. Also, we provide a simple versatile experimental platform to validate the theoretical results presented here by considering

stubs and segments made of standard coaxial cables operating in the radio-frequency domain. The existence of topological interface states is carried out from the dispersion relation and the symmetry of the band-edge states. This approach is equivalent to the determination of the Zak phases of the bulk bands for each of the PCs. Then, the existence and the position of such states are proved through (i) an investigation of the LDOS at the interface between two semi-infinite PCs, which is essential to determine Tamm states that appear as maxima in the LDOS inside the common gaps of the two PCs, (ii) the sign of the phase of the reflection coefficient at the boundary of each PC with a waveguide, and (iii) the scattering parameters (transmission and reflection coefficients as well as the phase of the determinant of the scattering matrix, the so-called Friedel phase) when two combined PCs are either attached horizontally inside a waveguide or grafted vertically along a waveguide. In addition, we provide closed-form expressions of the geometrical parameters and the frequency for which the interface state becomes a BIC. We show that these topological BICs are stationary states of the cavity between the two PCs, and are very robust to any perturbation on both sides of the cavity. Finally, we show the impossibility of existence of interface states between two PCs with identical periods and different stubs. The analytical calculations developed here are performed by means of the Green's function approach [62,63]. We recently adapted the theoretical approach to the case of acoustic waveguides [64] and it can be expected that the experimental observation of topological interface states can become possible in the future by means of side-coupled Helmholtz resonators [65]. For the sake of completeness, let us mention that preliminary theoretical results of the topological photonic interface states in comblike structures have been presented in a recent conference paper [66].

The outline of this paper is as follows: Considering PCs where the constitutive elements of each unit cell are monomode waveguides, we give in Sec. II a general theory of the dispersion relations of Tamm states between two semi-infinite and two finite PCs as well as the local and total DOS of two connected PCs made of symmetric cells. In Sec. III, we adapt the theory to the case of PC constituted by periodic stubs grafted along a waveguide and show numerical and experimental results for the effect of the periods on the existence of topological interface states in the case of NBC ($H = 0$) at the end of the stubs. Section IV shows the effect of the lengths of the stubs on the existence of topological interface states. In Sec. V, we give a summary of the main results of this work. The results of DBC ($E = 0$) at the end of the stubs are given in the Supplemental Material SM5 [67].

II. GENERAL THEORY OF BULK, SURFACE, AND INTERFACE STATES

In this section, we provide the main theoretical expressions that enable to derive the dispersion relations of infinite, semi-infinite, and finite PCs. Then, we show how one can deduce the dispersion relations of Tamm states between two semi-infinite and two finite PCs as well as the local and total DOS of two connected PCs. Also, we provide the analytical expressions of the transmission and reflection coefficients as well as the scattering matrix of two connected finite PCs. Finally, we give an exact relation between the phase of the determinant of the scattering matrix (the so-called Friedel phase [68]) and the total DOS. This general theory can be used by any reader interested in this domain for any 1D photonic crystal made of symmetric cells without going into details. It should be pointed out that the validity of our results is subject to the requirement that the propagation is monomode, i.e., the cross section of the waveguides is small compared to their length and to the propagation wavelength.

A. Dispersion relations of infinite, semi-infinite, and finite PCs

All the analytical calculations are performed in the framework of the Green's function method [63]. As mentioned before, in order to study topological Tamm states in 1D systems, we need the inverse of the Green's function of a symmetric unit cell [Fig. 1(a)] of PC1 in its space of interface $M = \{0, 1\}$,

$$g_{\text{cell}}^{-1}(M, M) = \begin{pmatrix} a_1 & b_1 \\ b_1 & a_1 \end{pmatrix}, \tag{1}$$

where a_1 and b_1 are real quantities. The details of these expressions will be given in Sec. III for a symmetric cell made of a stub of length d_1' placed in the middle of a segment of length d_1 [Fig. 1(a)].

The inverse of the Green's function of the infinite PC made of a periodic repetition of a given cell [Fig. 1(a)] is obtained from a linear superposition of the (2×2) matrix in Eq. (1) in the space of interfaces of all the sites n. We obtain a tridiagonal matrix where the diagonal and off-diagonal elements are given, respectively, by a_1 and b_1. Taking advantage of the Bloch theorem, the dispersion relation of the infinite periodic PC [Fig. 1(b)] is given by [28]

$$\cos\left(k_B^1 d_1\right) = -\frac{a_1}{b_1}, \tag{2}$$

where k_B^1 is the Bloch wave vector and d_1 is the period of the PC1.

For a semi-infinite PC1 terminated by a free surface [Fig. 1(c)], the inverse of the Green's function in the space at the surface {0} is given by [28]

$$g_{\text{PC1}}^{-1}(0, 0) = a_1 + b_1 t_1, \tag{3}$$

where $t_1 = \exp(k_B^1 d_1)$. Equation (3) can be written also in the form

$$g_{\text{PC1}}^{-1}(0, 0) = \frac{j\omega}{Z_1}, \tag{4}$$

where we introduce the surface impedance Z_1 of the PC1.

For a finite PC bounded by two surfaces $n = 0$ and N [Fig. 1(d)] with vanishing magnetic field ($H = 0$) on both sides, the inverse of the Green's function in the space of interfaces $M' = \{0, N\}$ is given by [28]

$$g_{\text{PC1}}^{-1}(M', M') = \begin{pmatrix} A_1 & B_1 \\ B_1 & A_1 \end{pmatrix}, \tag{5}$$

where

$$A_1 = (a_1 + b_1 t_1)\left(1 + t_1^{2N}\right) \tag{6}$$

and

$$B_1 = -b_1 t_1^N \left(t_1 - \frac{1}{t_1}\right). \tag{7}$$

B. Dispersion relations and local DOS of two connected PCs

Now, we consider two semi-infinite PCs connected in the space of interface $M_0 = \{0\}$ [Fig. 1(e)]. The inverse of the Green's function of the whole system in the interface space $\{0\}$ is given by [63]

$$g^{-1}(0,0) = g^{-1}_{\mathrm{PC1}}(0,0) + g^{-1}_{\mathrm{PC2}}(0,0). \tag{8}$$

The dispersion relation giving the interface states between two PCs is given by [63] $g^{-1}(0,0) = 0$ or equivalently using Eq. (4):

$$Z_1 + Z_2 = 0. \tag{9}$$

Equation (9) is the well-known matching impedance condition [41] that should be satisfied in order to realize interface states between two PCs.

The LDOS at the interface between two PCs is given by [62,63]

$$n(\omega) = \frac{2\omega}{\pi}\mathrm{Im}[g(0,0)] = \frac{2\omega}{\pi}\mathrm{Im}\left[\frac{g_{\mathrm{PC1}}(\omega^2)g_{\mathrm{PC2}}(\omega^2)}{g_{\mathrm{PC1}}(\omega^2)+g_{\mathrm{PC2}}(\omega^2)}\right]. \tag{10}$$

In order to calculate the eigenmodes of two connected finite PCs with $H = 0$ boundary condition on both sides [Fig. 1(f)], we need first to construct $g^{-1}(M'', M'')$ in the space of interfaces $M'' = \{-N, 0, N\}$ of the two connected PCs. From Eq. (5), we obtain

$$g^{-1}(M'', M'') = \begin{pmatrix} A_1 & B_1 & 0 \\ B_1 & A_1 + A_2 & B_2 \\ 0 & B_2 & A_2 \end{pmatrix}, \tag{11}$$

where A_2 and B_2 are given by the same expressions as in Eqs. (6) and (7) by changing the subscript 1 to 2. The eigenmodes of the two connected PCs in Fig. 1(f) are given by $\det[g^{-1}(M''M'')] = 0$ or, equivalently,

$$\rho = A_2\left(A_1^2 - B_1^2\right) + A_1\left(A_2^2 - B_2^2\right) = 0. \tag{12}$$

C. Scattering matrix parameters and total DOS

Here, we give the expressions of transmission and reflection coefficients and the reflection delay time as well as the phase of the determinant of the scattering matrix (the so-called Friedel phase [68]) and their relation to the variation of the DOS for two geometrical configurations depicted in Figs. 1(g) and 1(i).

(i) For the system in Fig. 1(g) where the two finite PCs are connected at their left extremity to only one semi-infinite waveguide, the inverse Green's function in the space of interfaces $M'' = \{-N, 0, N\}$ is given by

$$g_h^{-1}(M'', M'') = \begin{pmatrix} A_1 - jF & B_1 & 0 \\ B_1 & A_1 + A_2 & B_2 \\ 0 & B_2 & A_2 \end{pmatrix}, \tag{13}$$

where $-jF$ is the inverse Green's function of the semi-infinite waveguide. $F = \frac{\omega}{Z}$ where ω is the angular frequency and Z is the characteristic impedance of the waveguide.

The reflection coefficient for the system in Fig. 1(g) is given by [63]

$$r = -1 - 2jF g(-N,-N) = -\frac{\rho + j\tau}{\rho - j\tau}, \tag{14}$$

where ρ is defined in Eq. (12) and

$$\tau = A_2(A_1 + A_2) - B_2^2. \tag{15}$$

As predicted, for lossless system the incident wave is completely reflected $R = |r|^2 = 1$ [Eq. (14)]. However, for a lossy system a part of the energy is absorbed, then the reflection is no longer unity and the modes of the system appear as dips in the reflection spectra (see below).

In order to derive an analytic demonstration of the relation between the reflection delay time and the DOS, we consider the variation of the DOS between the two finite PCs and the semi-infinite waveguide [Fig. 1(g)] and a reference system made of decoupled semi-infinite waveguide and the two finite PCs. The variation of the DOS $[\Delta n(\omega)]$ is given by [63]

$$\begin{aligned}\Delta n(\omega) &= \frac{1}{\pi}\frac{d}{d\omega}\left\{\arg\left[\det\left(g_h^{-1}(M'', M'')\right)\right]\right\} \\ &= \frac{1}{\pi}\frac{d}{d\omega}\left[\arctan\left(\frac{\tau}{\rho}\right)\right].\end{aligned} \tag{16}$$

Another interesting quantity that can be extracted from the reflection coefficient is its phase delay time which represents the time taken by the electromagnetic wave to propagate through the structure [69]. It is defined as the first derivative of the phase time φ_R with respect to the frequency,

$$\tau_R = \frac{d\varphi_R}{d\omega} = 2\frac{d}{d\omega}\left[\arctan\left(\frac{\tau}{\rho}\right)\right]. \tag{17}$$

From Eqs. (16) and (17), one can deduce that for lossless system the DOS of the system is related to the reflection delay time by the relation

$$\tau_R = 2\pi\,\Delta n(\omega). \tag{18}$$

Let us mention that similar theoretical results can be obtained for the horizontal structure in Fig. 1(h). These results are given in Supplemental Material SM4 [67].

(ii) For the vertical structure [Fig. 1(i)], the two finite PCs are grafted at the same site $\{-N\}$ along an infinite waveguide. The inverse of the Green's function of the vertical structure in the space of interfaces $M'' = \{-N, 0, N\}$ becomes

$$g_v^{-1}(M'', M'') = \begin{pmatrix} A_1 - 2jF & B_1 & 0 \\ B_1 & A_1 + A_2 & B_2 \\ 0 & B_2 & A_2 \end{pmatrix}. \tag{19}$$

From Eq. (19), one can deduce the transmission and reflection coefficients for the vertical structure as follows:

$$t_v = -2jF g_v(-N,-N) = -\frac{2j\tau}{\rho - 2j\tau}, \tag{20}$$

$$r_v = -1 - 2jF g_v(-N,-N) = -\frac{\rho}{\rho - 2j\tau}, \tag{21}$$

where ρ and τ are given by Eqs. (12) and (15).

It is worth mentioning that the zeros of transmission and reflection give a direct access to the eigenmodes of the finite vertical structure attached to the waveguide. Indeed, the eigenmodes of the finite PC with $E = 0$ boundary condition at the bottom side and $H = 0$ boundary condition at the top side of the structure are given by $\tau = 0$ [70] which is equivalent to vanishing the transmission t_v [Eq. (20)]. Similarly, the eigenmodes of the two finite PCs with $H = 0$ on both sides of the

structure are given by $\rho = 0$ [70] which is equivalent to the maxima of the transmission amplitude [Eq. (20)].

D. Conditions for BICs

BICs are obtained from vanishing both the real and imaginary parts of the poles of the Green's function or equivalently from canceling the denominators of both the transmission and reflection coefficients. These BICs are common modes between the three configurations in Figs. 1(g), 1(h), and 1(i) and are independent of the semi-infinite media (continuum) in contact with the two connected finite PCs. One can see that a simple analytical solution which enables to cancel simultaneously the real and imaginary parts of the denominators of all the transmission and reflection coefficients obtained above [Eqs. (14), (20), and (21)] is given by $B_1 = 0$, $B_2 = 0$, and $A_1 + A_2 = 0$. From Eqs. (6) and (7), these three conditions are equivalent to

$$b_1 = 0,\ b_2 = 0, \quad \text{and} \quad a_1 + a_2 = 0. \tag{22}$$

III. THEORETICAL AND EXPERIMENTAL EVIDENCE OF TOPOLOGICAL TAMM STATES IN PHOTONIC STUBBED STRUCTURES

The purpose of this section is to demonstrate the existence of topological Tamm states at the interface between two semi-infinite and two finite PCs and discuss their behaviors in the different scattering parameters such as the transmission and reflection coefficients as well as the Friedel phase and DOS. The PCs are composed of periodic symmetric cells [Fig. 1(a)] with different geometrical parameters for each PC. The unit cell is made of a stub of length d_i' grafted in the middle of a segment of length d_i [Fig. 1(a)]. Neumann boundary condition ($H = 0$) is applied at the free end of the stubs. Similar results for Dirichlet boundary conditions ($E = 0$) are presented in the Supplemental Material SM5 [67].

With the help of the Green's function approach [63], the analytical expressions of a_i and b_i in Eq. (1) are given by (for more details see the Supplemental Material SM1 [67])

$$a_i = \frac{-F[2C_iC_i' + S_iS_i']}{2S_i''[2C_i'C_i'' + S_i'S_i'']} \tag{23}$$

and

$$b_i = \frac{FC_i'}{S_i''[2C_i'C_i'' + S_i'S_i'']}, \tag{24}$$

where $C_i = \cos(kd_i)$, $S_i = -j\,\sin(kd_i)$, $C_i' = \cos(kd_i')$, $S_i' = -j\,\sin(kd_i')$, $C_i'' = \cos(k\frac{d_i}{2})$, $S_i'' = -j\,\sin(k\frac{d_i}{2})$ $(i = 1, 2)$. $k = \frac{\omega\sqrt{\varepsilon}}{c}$ is the wave vector, $F = \frac{-j\omega}{Z}$, and $j = \sqrt{-1}$. ω is the angular frequency, ε is the permittivity of the waveguide, and Z its characteristic impedance.

From Eqs. (2), (23), and (24), one can obtain the dispersion relation of the infinite periodic PC,

$$\cos\left(k_B^i d_i\right) = C_i + \frac{1}{2}\frac{S_iS_i'}{C_i'}. \tag{25}$$

Also, from Eqs. (22), (23), and (24), one can deduce easily an analytical expression giving the BICs, namely,

$$\cos(kd_1') = 0,\ \cos(kd_2') = 0,\ \text{and}\ \sin\left(k\left[\frac{d_1 + d_2}{2}\right]\right) = 0. \tag{26}$$

In this section, we will fix $d_1' = d_2' = 1$ as the unit of length and vary the periods d_1 and d_2. In this case, Eq. (26) enables to fix the relationship that should be satisfied between the geometrical lengths of the system and the BIC frequency, namely,

$$\frac{d_1 + d_2}{d_1'} = \frac{4n}{(2n' + 1)} \tag{27}$$

and

$$\Omega = \frac{kd_1'}{\pi} = \frac{(2n' + 1)}{2}, \tag{28}$$

where n and n' are integers. The BIC corresponds to a standing mode of a cavity consisting of the segment of length $\frac{d_1+d_2}{2}$ at the interface surrounded by two stubs of length d_1' such that the electric field in the eigenfunction vanishes at the connection points of the segment and the stubs. This mode is independent of the number of cells N in the PCs as well as on the semi-infinite waveguides.

A. Theoretical results: Interface states from Zak phases and sign of the reflection phases

In 1D periodic systems, the Zak phase of a given band is defined as [38,39]

$$\theta_n^{\text{Zak}} = \int_{-\pi/d_1}^{\pi/d_1}\left[i\int_{\text{unit cell}} dx\,\varepsilon(x)u_{n,q}^*(x)\partial_q u_{n,q}(x)\right]dq, \tag{29}$$

where x represents the spatial coordinate, $\varepsilon(x)$ is the relative permittivity, and $u_{n,q}$ is the normalized periodic part of the electric-field Bloch wave eigenfunction with a given wave vector q. Aside from the analytical calculation based on the Bloch eigenfunctions [Eq. (29)], the Zak phase can also be determined from the symmetry of the band-edge states [38]. If the unit cell admits an inversion symmetry and the origin of coordinate is fixed at the symmetry center, the Zak phase calculated from Eq. (29) can take only two defined values, 0 or π [38,41]. If the electric field at the band edges of a given band has identical symmetry such as both are symmetric or antisymmetric, the Zak phase of this band is 0. Otherwise, the Zak phase is π.

In order to demonstrate the existence of topological interface states and their properties in our PC, we analyze first the dispersion relation of an infinite PC made of periodic symmetric cells, where each unit cell is formed out by a stub of length d_1' and a period of length d_1 [Fig. 1(a)]. All the lengths are taken in units of d_1'. In Fig. 2(a), we plot the band-gap structure of an infinite PC as a function of the period d_1 and the dimensionless frequency $\Omega = \frac{\omega d_1'}{c\pi}\sqrt{\varepsilon}$. One of the advantages of the comblike structure is the fact that it can present two types of gaps: Bragg gaps originating from the periodicity of the crystal and hybridization gaps originating from local resonances of the grafted stubs. It can be seen the existence of band-crossing points which represent the position of the flat bands (FBs). These FBs are obtained from the dispersion

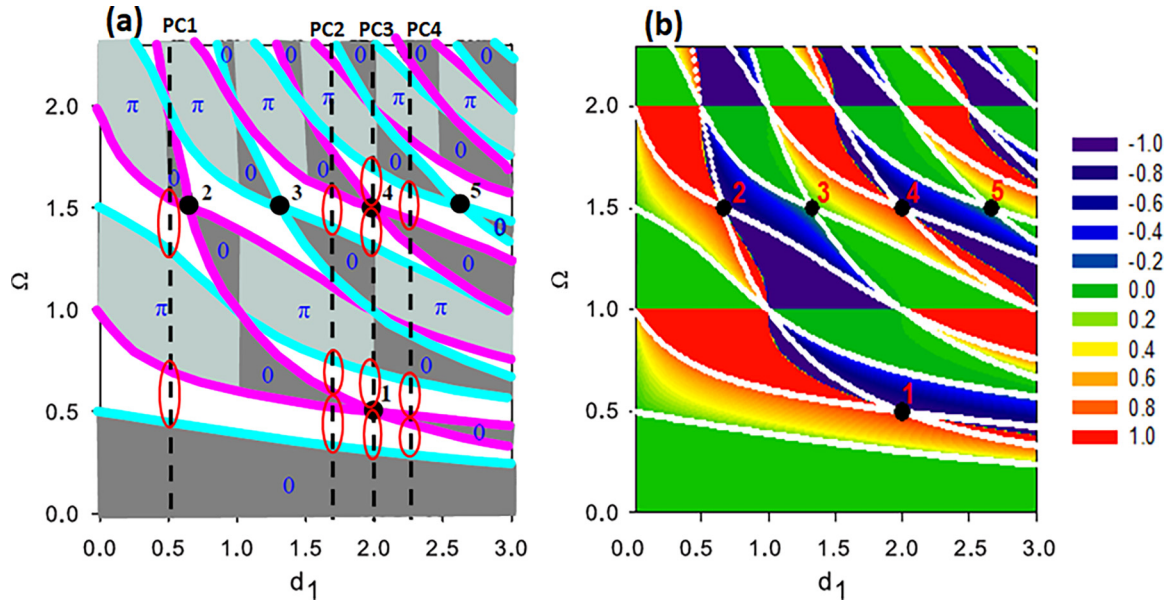

FIG. 2. (a) Band-gap structure of an infinite PC made of symmetric unit cells in Fig. 1(a) as a function of the length d_1 and Ω for fixed $d_1' = 1$ (considered as the unit of length) with NBC at the end of the stubs. The black dots 1 to 5 indicate the band-crossing points where the bands close and reopen. Pink and cyan colors indicate the symmetric and antisymmetric band-edge states, respectively. Gray and dark cyan colors give the bands for which the Zak phase is 0 and π, respectively. (b) Reflection phase at the boundary of a semi-infinite PC with a waveguide as a function of d_1. The colors indicate the reflection phase (in units of π), which vary from -1 to 1. White lines give the limits of the bulk bands.

relation [Eq. (25)] when both its numerator and denominator vanish together, namely, $S_1 = 0$ (i.e., $\frac{\omega d_1}{c}\sqrt{\varepsilon} = m_1\pi$) and $C_1' = 0$ [i.e., $\frac{\omega d_1'}{c}\sqrt{\varepsilon} = (2m_1' + 1)\frac{\pi}{2}$], where m_1 and m_1' being integers. Therefore, the flat bands are given by

$$\frac{d_1}{d_1'} = \frac{2m_1}{2m_1' + 1}, \tag{30}$$

and the dimensionless frequency

$$\Omega = m_1' + \tfrac{1}{2}. \tag{31}$$

Black dots labeled 1 to 5 in Fig. 2(a) indicate the positions of the band crossing (flat bands) where the bands close and reopen. They correspond to the pairs $(m_1, m_1') = (1, 0), (1, 1), (2, 1), (3, 1), (4, 1)$, respectively. The flat bands appearing at higher frequencies (larger m_1') are not presented. To predict the existence of topological interface states in a common gap of two PCs, we use the symmetry of the electric field at the band-edge states. It is known [38] that if the lower (or upper) band-gap edges of the two PCs have opposite symmetries, the common gap must support an interface state. This approach is equivalent to using the Zak phases of the bulk bands which can be also identified from the symmetry of the edge states as mentioned above. The symmetry of the band-edge states for our PC as function of d_1 is represented by pink and cyan colors in Fig. 2(a) for symmetric and antisymmetric states, respectively. Also, the Zak phases of the bulk bands are indicated by gray and dark cyan colors for 0 and π, respectively.

It can be seen that near to the band-crossing points (labeled 1 to 5) the band-edge states exhibit the same symmetry, due to the existence of flat bands. This property ensures that if we take two PCs with different values of d_1 on both sides of these points, such as the upper edge state of the first PC and the lower edge state of the second PC exhibit the same symmetry, the common gap between them must necessarily support an interface state. For example, consider two PCs around the point 4 with different values of d_1 such as $d_1 = 1.7$ and $d_1 = 2.3$ [labeled PC2 and PC4 in Fig. 2(a)]. It is clear that passing through the band-crossing point (labeled 4) the upper edge state of the first PC becomes the lower edge state of the second PC with the same symmetry (both symmetric), thus, the common gap between these two PCs around $\Omega = 1.5$ should necessarily support an interface state. This rule can be applied around all other band-crossing points for the lower and upper common gaps around $\Omega = 0.5$ and 1.5, respectively. In addition, another interesting point happens when, at a given frequency ($\Omega = 1.5$ in the following), we associate two PCs at the values of d_1 where the flat bands occur, namely, points 2, 3, 4, and 5 in Fig. 2(a). Indeed, a pair of PCs will exhibit two consecutive common gaps separated by a flat band. And, if the corresponding flat bands have different parities, then one interface state appears in each of the two consecutive common gaps. This statement holds for the pairs (2-3), (2-5), (3-4), and (4-5). All these points will be explained in more details in Figs. 3 and 9 below.

In addition to the symmetry of the bulk-edge modes, another way to predict the existence of topological interface states is based on considering the signs of the phase of the reflection coefficient at the boundary of each semi-infinite PC [Fig. 1(c)] with a homogeneous waveguide characterized by the impedance Z [i.e., $g^{-1}(\omega^2) = \frac{j\omega}{Z}$]. Indeed, the reflection coefficient is given by

$$r_i = \frac{Z_i - Z}{Z_i + Z}\ (i = 1, 2). \tag{32}$$

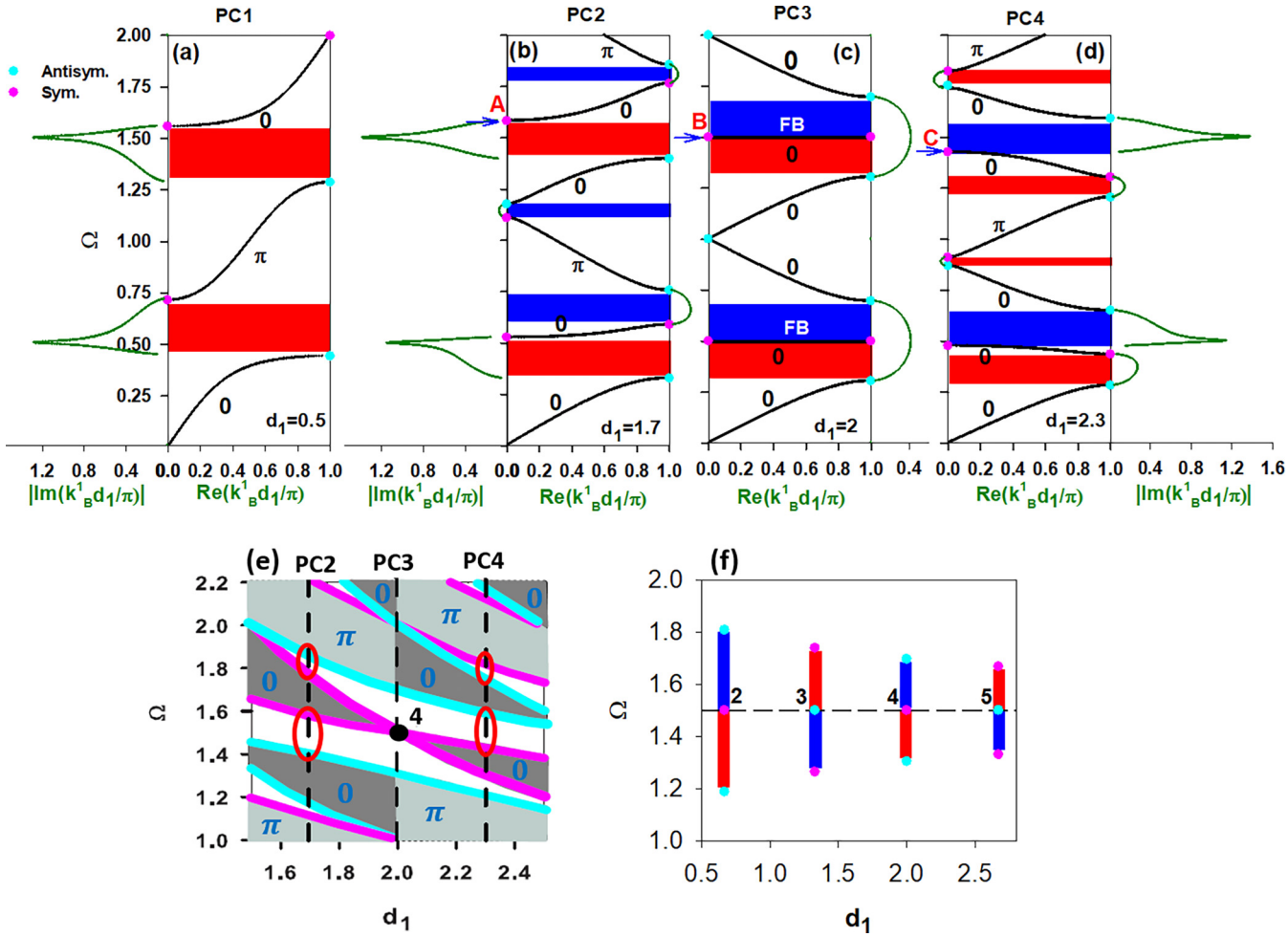

FIG. 3. (a)–(d) Band-gap structures for four PCs with different values of d_1: 0.5, 1.7, 2, and 2.3 corresponding to PC1, PC2, PC3, and PC4, respectively, in Fig. 2(a). Black and green curves give the real and imaginary parts of the Bloch wave vector in the first Brillouin zone. The Zak phases of each bulk band are labeled by 0 or π. The pink and cyan dots represent the symmetric and antisymmetric band-edge states, respectively. The gaps are colored in blue or red depending on whether the sign of the reflection phase is negative or positive. (e) Zoom around the band-crossing point 4 in Fig. 2(a). (f) Band-edge states for four PCs at the flat bands labeled 2, 3, 4, and 5 in Fig. 2(a) at $\Omega = 1.5$.

From Eq. (32), one can obtain

$$Z_i = Z\left(\frac{1-r_i}{1+r_i}\right). \tag{33}$$

Therefore, Eqs. (9) and (33) enable to get the condition $r_1 r_2 = 1$ for the existence of an interface state at the boundary of the two PCs. This condition is equivalent to $|r_1||r_2| = 1$ and

$$\phi_{\mathrm{PC1}} + \phi_{\mathrm{PC2}} = 0. \tag{34}$$

Figure 2(b) gives the reflection phase (in color scale) at the boundary of a semi-infinite PC [Fig. 1(c)] with a waveguide as function of the length d_1 and the dimensionless frequency Ω. White lines indicate the limits of the bulk bands. The colors represent the reflection phase (in units of π), which vary from -1 to 1. Red and blue colors in the gaps correspond to $\mathrm{sgn}(\phi_n) > 0$ and $\mathrm{sgn}(\phi_n) < 0$, respectively. This approach can be used to predict the existence of topological interface states by satisfying Eq. (34) and confirm the results in Fig. 2(a) obtained from the symmetry of the band-edge modes. A topological interface state must exist in a common gap if the signs of the reflection phases of two PCs are opposite, i.e., the gaps take different colors. It is clear that the gaps around the crossing points (labeled 1 to 5) have different signs of the reflection phase. Therefore, it is sufficient to take two PCs with common gaps and opposite phase reflections to get an interface state.

Let us mention that the sign of the reflection phase of the nth gap can be also deduced from the Zak phase of the bands below this gap using the following equation [38]:

$$\mathrm{sgn}(\phi_n) = (-1)^{n+1} \exp\left(i \sum_{m=1}^{n-1} \theta_m^{\mathrm{Zak}}\right). \tag{35}$$

Therefore, the Zak phase of the bands enables us to show the possibility of interface states between two PCs based on the sign of the reflection phase in each gap [Eq. (35)].

From Eq. (35), one can show easily that the Zak phase of the nth bulk band can be derived from the sign of the reflection phases ϕ_n and ϕ_{n-1} of the nth and $(n-1)$th gap surrounding the nth band using the relation [38,40,41]

$$\exp\left(i\theta_n^{Zak}\right) = -\frac{\mathrm{sgn}\,(\phi_n)}{\mathrm{sgn}\,(\phi_{n-1})}. \tag{36}$$

TABLE I. Existence or nonexistence of topological interface states deduced from the band-edge symmetries for all possible combinations between the four PCs in Figs. 3(a)–3(d).

Common gaps	PC1-PC2	PC1-PC3	PC1-PC4	PC2-PC3	PC2-PC4	PC3-PC4
Gap 4		Yes		Yes	Yes	No
Gap 3	No	No		No	Yes	Yes
Gap 2	Yes	Yes	Yes	No	No	No
Gap 1	No	No	Yes	No	No	No

In order to give a better idea about the possible combinations of PCs to get topological interface states, we plot in Figs. 3(a)–3(d) the band structures in the first Brillouin zone for four PCs with different values of d_1 selected by vertical dashed lines in Fig. 2(a). The four PCs are chosen in such a way as to find large common gaps between them and to get topological interface states around the band-crossing points 1 and 4 in the lower and upper common gaps around $\Omega = 0.6$ and 1.5, respectively. In Figs. 3(a)–3(d), the real part of the Bloch wave vector within the first Brillouin zone is plotted by black curves, while its imaginary part is given by green curves inside the gaps. The symmetric and antisymmetric band-edge modes are given by pink and cyan colors, respectively. Also, the Zak phase of each band is noted as 0 or π. Based on the symmetry argument, one can predict the existence of topological interface states in the common gaps for the different combinations of the four PCs (1 to 4) in Fig. 2(a). For example, for the pair PC1-PC2 [Figs. 3(a) and 3(b)], there exist three common gaps around $\Omega = 0.5$, 0.7, and 1.5. One can predict that the second common gap around $\Omega = 0.7$ may support an interface state since the lower and upper edge states at this gap have opposite symmetries. In contrast, there is no interface state in the first and third common gaps around $\Omega = 0.5$ and 1.5 because the lower (respectively upper) edge states of the corresponding gaps have the same symmetry, i.e., they are both antisymmetric (respectively symmetric). The same symmetry argument allows us to conclude the existence or nonexistence of topological interface states between the five other combinations between PC1, PC2, PC3, and PC4. These conclusions are summarized in Table I.

In addition, the signs of the reflection phases in the gaps for the four PCs are deduced from Fig. 2(b) and indicated in Figs. 3(a)–3(d) by red and blue colors corresponding to $\mathrm{sgn}(\phi_n) > 0$ and $\mathrm{sgn}(\phi_n) < 0$, respectively. As mentioned before, from the sign of the reflection phases, it is sufficient to take two PCs with different signs (different colors) in their common gaps to get a topological interface state. All the conclusions deduced from the sign of the reflection phases are in accordance with those summarized in Table I.

To give a better insight about the edge modes symmetry inversion process around the flat bands, proposed here to display the possibility of topological interface states, we focus on three band structures in Figs. 3(b)–3(d) around the flat band labeled 4 in Fig. 2(a) and magnified in Fig. 3(e). One can see that the band just above $\Omega = 1.5$ in Fig. 3(b) ($d_1 = 1.7$) with positive group velocity ($V_g = \frac{d\omega}{dk_B} > 0$) becomes flat for $d_1 = 2$ and $\Omega = 1.5$ in Fig. 3(c) ($V_g = 0$) and then its slope becomes inverted just below $\Omega = 1.5$ in Fig. 3(d) for $d_1 = 2.3$ ($V_g < 0$). All these bands are characterized by the same symmetry at their edges (here symmetric). Therefore, the symmetry of the upper band-edge mode for PC2 at $d_1 = 1.7$ [labeled A in Fig. 3(a)] and the lower band-edge mode for PC4 [labeled C in Fig. 3(d)] for $d_1 = 2.3$ are the same. This is due to the existence of the flat band at $\Omega = 1.5$ for $d_1 = 2$ that exhibits the same symmetry at its band edges [labeled B in Fig. 3(b)]. This property is sufficient to ensure that two PCs chosen around the flat band should present a common gap that must support a topological interface state. In addition to the common gap of hybridization type around $\Omega = 1.5$ for PC2 and PC4, there exists a common Bragg gap type around $\Omega = 1.8$ [Figs. 3(b) and 3(d)] which must also support an interface state. These common gaps must support an interface state since their lower and upper edge states have opposite symmetries. In Figs. 3(a)–3(d), we give by green curves the imaginary parts of the Bloch wave vector in the gaps. It can be seen that the imaginary part diverges inside the hybridization gap at the frequency of the flat band ($\Omega = 1.5$) while it remains finite in the Bragg gap around $\Omega = 1.8$. This means that the interface state falling within the hybridization gap is more localized than the one appearing inside the Bragg gap. This represents an advantage of our proposed PC in comparison with those based on only Bragg gaps. Another interesting idea consists in considering two PCs characterized by two common gaps with a flat band falling in the middle, but with different symmetries; this is the case for PCs at points (2,3), (2,5), (3,4), and (4,5) in Fig. 2(a) around $\Omega = 1.5$. Indeed, any combination of these two PCs gives rise to two topological interface states in two successive common gaps separated by a flat band. This result is better explained in Fig. 3(f) where we have plotted the band-edge modes with their symmetries for the flat bands 2 to 4 in Fig. 2(a). The common gaps between the successive PCs decrease as a function of d_1. Obviously, based on the symmetry argument or on the sign of the reflection phase one can obtain two topological interface states if we combine two PCs at the flat bands (2,3), (2,5), (3,4), and (4,5).

B. Theoretical results: Interface states from dispersion relation and local density of states

Now, we analyze the existence of interface states through the dispersion curves and the LDOS of two connected semi-infinite PCs [Fig. 1(e)]. The first and second PCs are characterized by periods of lengths d_1 and d_2 and stubs of lengths d_1' and d_2', respectively, with $d_1' = d_2' = 1$. To this end, we have fixed the length of the first PC at $d_1 = 0.5$ and vary the length of the second period d_2. Figure 4(a) shows the projected band structure as a function of d_2 and Ω. The values of d_2 have been chosen to discuss the topological interface states in the lower and upper common gaps around $\Omega = 0.6$ and 1.5, respectively. The shaded areas in Fig. 4(a) represent

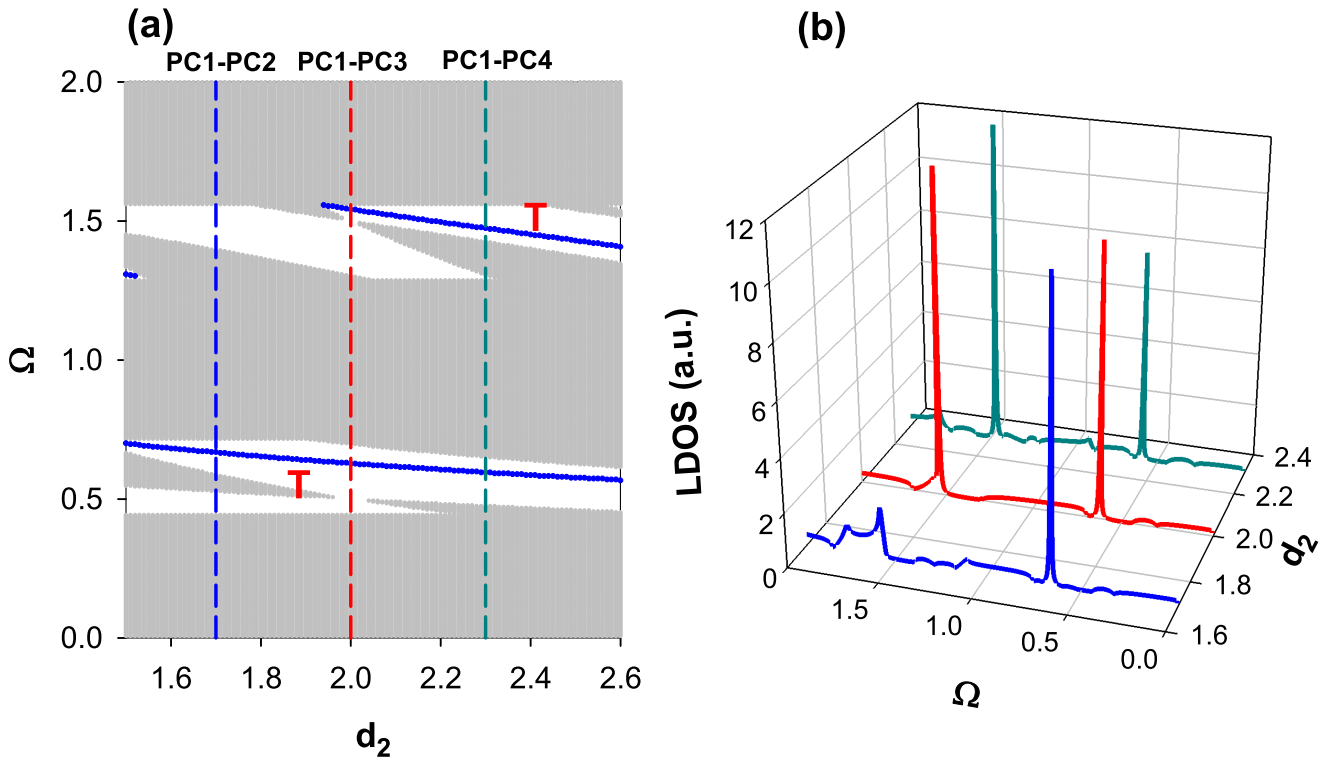

FIG. 4. (a) Projected band-gap structure and interface states between two semi-infinite PCs as a function of the period d_2 of the second PC. The other lengths are fixed at $d_1 = 0.5$, $d_1' = d_2' = 1$. The shaded areas represent the bulk bands, while white areas show the common gaps of the two PCs. The blue branches indicate the localized interface states. (b) LDOS spectra versus Ω for three values of d_2 such as $d_2 = 1.7$, $d_2 = 2$, and $d_2 = 2.3$ indicated by dashed vertical lines in (a).

the bulk bands, while the white areas display the common gaps of the two PCs. The blue branches inside the common gaps indicate the positions of localized Tamm states obtained from the maxima of the LDOS [Eq. (10)]. The existence and the position of localized interface states vary as a function of d_2. The frequencies of the localized Tamm states decrease as d_2 increases until they merge in the bulk bands and become resonant states. This plot gives us a map about the existence of localized Tamm states between two semi-infinite PCs. Figure 4(b) illustrates three examples of LDOS spectra as a function of Ω for three values of d_2 such as $d_2 = 1.7$ (PC2), $d_2 = 2$ (PC3), and $d_2 = 2.3$ (PC4) indicated by vertical dashed lines in Fig. 4(a). Obviously, the Tamm states appear as well-defined peaks inside the common gaps of the two PCs, their frequency positions depend on the value of d_2. These results are in accordance with those predicted in Table I (see the first three columns). In the following two subsections, we will give an experimental validation of all the theoretical results discussed above by considering two connected finite PCs either attached to one semi-infinite waveguide [Fig. 1(g)] or grafted vertically at one point of a horizontal waveguide [Fig. 1(i)].

C. Experimental results: Horizontal structure

In this section, we will give first an experimental demonstration of the Zak phase of the bulk bands for three PCs: PC1, PC2, and PC4 in Figs. 2(a) and 3(a), 3(b), and 3(d). For this reason, we consider the total reflection configuration depicted in Fig. 1(g). As mentioned in Sec. II C, the reflection rate is unity for lossless system [Eq. (14)]; however, as demonstrated in Sec. III A the sign of the phase of the reflected wave of two successive gaps surrounding a given band can inform us about the Zak phase of this band [Eq. (36)].

Figures 5(a), 5(b), and 5(f) show the numerical (green curves) and experimental (open circles) reflection phases of PC1, PC2, and PC4, respectively. The gray areas show the gaps of each PC. The lengths of the stubs are chosen such that $d_1' = d_2' = 1$ m. The details of the experimental setup used here are given in the Supplemental Material SM2 [67]. The $E = 0$ boundary condition corresponds to short-circuit termination at the end of the stubs, while the $H = 0$ boundary condition corresponds to open-circuit termination (see Fig. S2 [67]). For the considered losses in coaxial cables, the latter equation [Eq. (36)] remains valid and enables us to deduce the experimental Zak phases and to predict the existence of topological interface states. From the sign of the reflection phases in the gaps, we can deduce the Zak phase of each band using Eq. (36). These results are reported in Table II and confirm the theoretical predictions in Figs. 3(a), 3(b), and 3(d) for PC1, PC2, and PC4, respectively.

Now, from the phases ϕ_{PC1} and ϕ_{PC2} of PC1 and PC2 [Figs. 5(a) and 5(b)], one can predict the position of the interface state falling in their common gaps when these two PCs are connected together using Eq. (34) of phase matching (i.e., $\phi_{PC1} + \phi_{PC2} = 0$). The vertical arrows in Figs. 5(a) and 5(b) show the frequency ($\Omega = 0.66$) where the latter equation is fulfilled in the second common gap. In order to give an

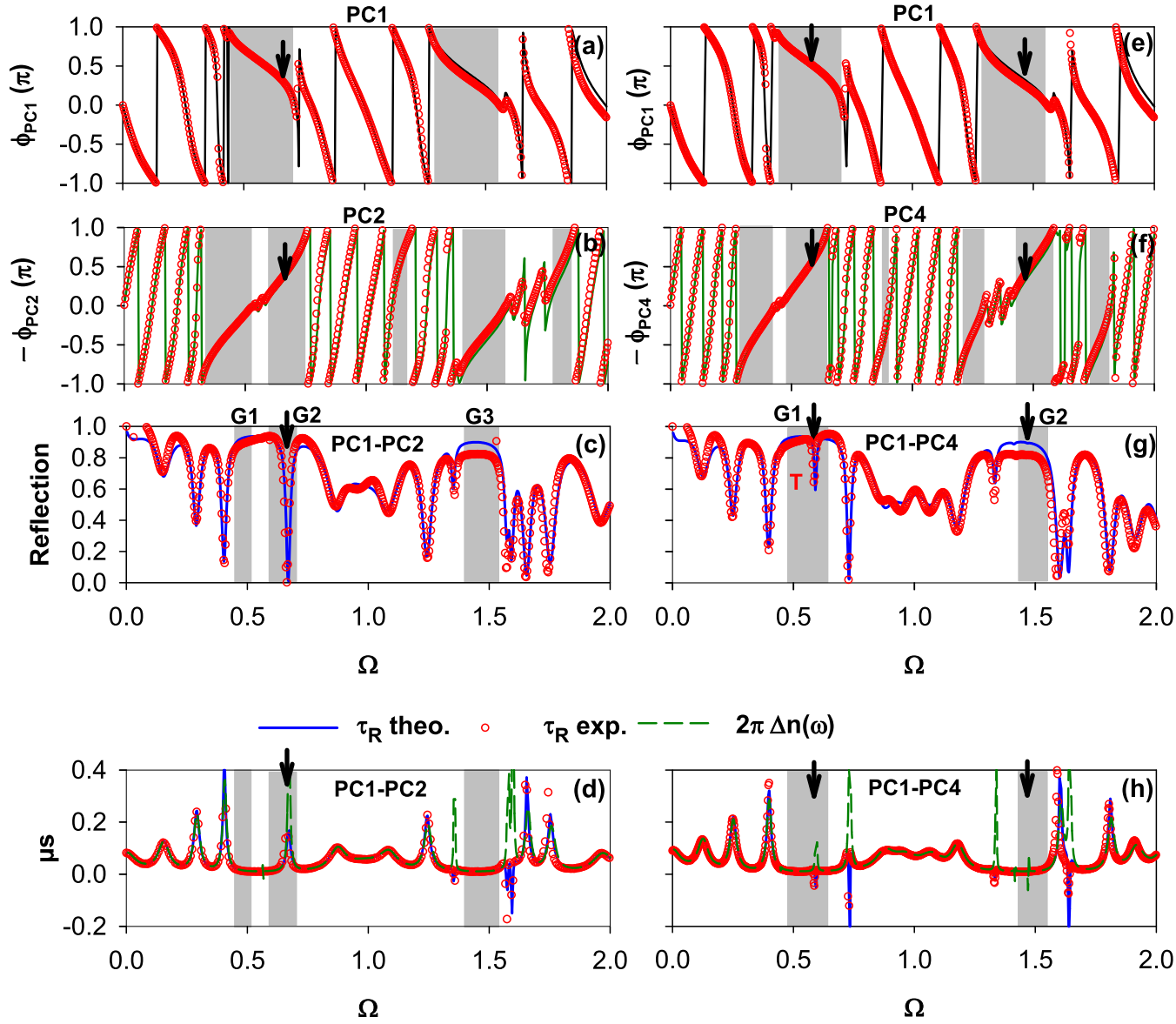

FIG. 5. (a) Reflection phase of PC1 with $d_1 = 0.5$ as a function of Ω. (b) Minus the reflection phase of PC2 with $d_1 = 1.7$ as a function of Ω. (c) Reflection amplitude for a finite PC made of PC1-PC2 as a function of Ω. (d) Reflection delay time and the variation of DOS $[2\pi\,\Delta n(\omega)]$ as a function of Ω for a finite PC made of PC1-PC2. Solid lines represent the theoretical results in presence of loss, while open circles give the experimental measurements. Green dashed curves give the variation of the DOS. (e)–(h) Same as (a)–(d) but for PC1 ($d_1 = 0.5$) and PC4 ($d_1 = 2.3$). The gray areas in (a), (b), (e), and (f) indicate the gaps of each PC, while the gray areas in (c), (d), (g), and (h) represent the common gaps between each combination of PCs: PC1-PC2 and PC1-PC4. The arrows indicate the position of the topological interface states.

experimental validation of this result, we plotted in Fig. 5(c) the reflection spectrum for two finite PCs (PC1-PC2), each one is composed of $N = 2$ stubs. One can see clearly the existence of a dip in the second common gap (labeled G2) at $\Omega = 0.66$ which is a signature of the interface Tamm state. As mentioned previously, without loss the amplitude of the reflection is unity, however, in presence of loss the modes of the two PCs appear as dips in the reflection amplitude. The intensity of the reflection dips depends on the strength of loss in the system; in our case the reflection amplitude almost vanishes at $\Omega = 0.66$ giving rise to a near perfect absorption at this frequency [71,72].

This result is also confirmed by the reflection delay time in Fig. 5(d) which provides a clear signature of the topological interface state inside the second common gap; however, there is no interface state in the first and third common gaps. We have checked that in lossless and low-loss systems the phase of the two connected PCs vanishes (i.e., $\phi_{\text{PC1-PC2}} = 0$) at the same frequency. However, for high losses which go beyond the coaxial cable structure, the latter relation is no longer valid but the interface state gives a signature in the reflection delay time of the two connected PCs [Fig. 5(d)]. This result can be also obtained in the total DOS (green dashed lines) which shows almost the same behavior as the reflection delay time despite the presence of loss. In the absence of loss, the variation of the DOS is identical to the reflection delay time [Eq. (18)]. For low-loss systems, these two latter quantities remain approximately equivalent [69]. However, for

TABLE II. Experimental Zak phases of PC1, PC2, and PC4 deduced from Figs. 5(a), 5(b), and 5(f).

PC1			PC2			PC4		
Band/gap	Sign of the reflection phase	Zak phase	Band/gap	Sign of the reflection phase	Zak phase	Band/gap	Sign of the reflection phase	Zak phase
						Band 7		π
						Gap 6	+	
			Band 6		π	Band 6		0
			Gap 5	−		Gap 5	−	
			Band 5		0	Band 5		0
			Gap 4	+		Gap 4	+	
			Band 4		0	Band 4		π
			Gap 3	−		Gap 3	+	
Band 3		0	Band 3		π	Band 3		0
Gap 2	+		Gap 2	−		Gap 2	−	
Band 2		π	Band 2		0	Band 2		0
Gap 1	+		Gap 1	+		Gap 1	+	
Band 1		0	Band 1		0	Band 1		0

high losses the DOS and the reflection delay time exhibit different behaviors at some frequencies where the latter changes sign and appears as negative delta peak in the reflection delay time. The DOS represents an essential quantity to study and measure the modes of the system in particular topological interface modes [73].

Similar results are found for PC1 ($d_1 = 0.5$) and PC4 ($d_2 = 2.3$) [Figs. 5(e) and 5(f)] for the Zak phases of the bands (see Table II). However, in this case, one can predict topological interface states for PC1-PC4 both in the first and second common gaps since the condition $\phi_{PC1} + \phi_{PC4} = 0$ is satisfied in these two gaps as shown by the vertical arrows at $\Omega = 0.58$ and 1.6 in Figs. 5(e) and 5(f), respectively. Now, by associating in tandem these two PCs [Fig. 5(g)], one can see that the lower interface mode at $\Omega = 0.58$ in the first common gap (denoted G1) appears as a dip in the reflection spectrum, however, the upper interface mode at $\Omega = 1.6$ in the second common gap (denoted G2) did not give any signature in the reflection spectrum [Fig. 5(g)]. Indeed, this mode falls at the vicinity of the BIC given by Eqs. (27) and (28), namely, $d_2^{BIC} = 2.16$ and $\Omega_{BIC} = 1.5$ for $n = 2$ and $n' = 1$. Therefore, its width is very small which prevents its experimental observation due to the absorption in the cables. The existence and frequency of the experimental topological interface states for the combinations PC1-PC2 and PC1-PC4 are given in Table III. The frequencies of these interface modes are quite similar to those found theoretically in Fig. 4(a) for the interface between two semi-infinite PCs: PC1-PC2 and PC1-PC4.

TABLE III. Existence and frequency of experimental topological interface states for the two combinations PC1-PC2 and PC1-PC4 in Figs. 5(c) and 5(g), respectively.

	Interface state (Ω)	
Common gaps	PC1-PC2	PC1-PC4
Gap 3	No	
Gap 2	Yes ($\Omega = 0.66$)	Yes ($\Omega = 1.6$)
Gap 1	No	Yes ($\Omega = 0.58$)

In order to show the evolution of the interface modes and their quality factors around the two BICs mentioned before, we have plotted in Fig. 6(a) some spectra of the DOS around $d_2^{BIC} = 2.16$ and $\Omega_{BIC} = 1.5$. Obviously, for $d_2 = 2$ and 2.1, the topological interface state appears as well-defined peak in the DOS spectra, its width decreases as d_2 increases giving rise to a topological BIC at $d_2^{BIC} = 2.16$ and $\Omega_{BIC} = 1.5$ (indicated by a vertical arrow). This mode is given by Eqs. (27) and (28) for $n = 2$ and $n' = 1$. For $d_2 > d_2^{BIC}$, the peak reappears again at $\Omega < 1.5$. In Fig. 6(b), we have presented the quality factor as a function of d_2 around the topological BIC obtained from the peaks in the DOS spectra in Fig. 6(a). One can notice that the quality factor depends on d_2 and reaches a high value when d_2 tends to d_2^{BIC}. For d_2^{BIC}, the quality factor diverges to infinity giving rise to a topological BIC.

Figure 7(a) shows a better insight about the evolution of the modes of the horizontal configuration depicted in Fig. 1(g) as a function of d_2 and Ω for fixed $d_1 = 0.5$ and $d_1' = d_2' = 1$. The shaded areas show the bulk bands of the infinite systems, while the white areas represent the common gaps as function of d_2. The modes are deduced from the minima of the reflection amplitude in the reflection spectra as depicted in Figs. 5(c) and 5(g) (see also Fig. S3 in Supplemental Material SM3 [67]). In Fig. 7(a), we reported the minima of the reflection amplitude for two finite PCs, each one being made of $N = 2$ stubs. Within the common gaps (white areas), the blue branches represent the topological interface states. Open circles give the experimental measurements which reproduce very well the theoretical results inside the bulk bands and within the lower common gap around $\Omega = 0.6$, while the modes inside the upper common gap around $\Omega = 1.5$ are not detected. This is again due to the proximity of the interface state with the BIC which makes its observation difficult due to the losses in the coaxial cables. These modes can be also deduced from the peaks of the reflection delay time spectra for different values of d_2 [see Figs. 5(d) and 5(h) and also Fig. S3 in Supplemental Material SM3 [67]). Despite the small number of cells considered ($N = 2$), these results give an experimental validation of the theoretical results discussed

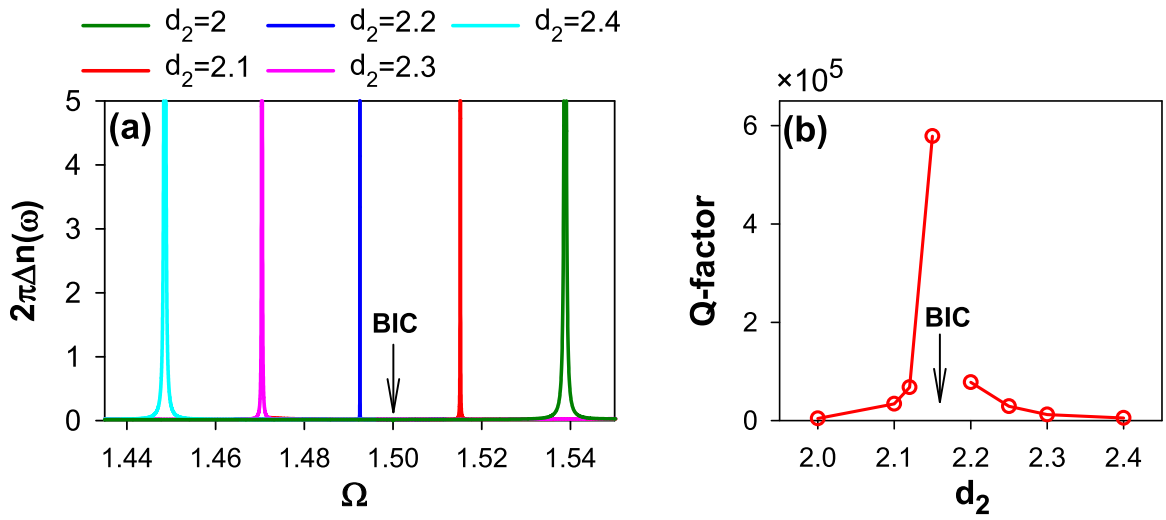

FIG. 6. (a) DOS spectra for certain values of d_2 around the topological BIC that falls in the upper common gap around $\Omega_{\rm BIC} = 1.5$. The BIC falls at $\Omega_{\rm BIC} = 1.5$ for $d_2^{\rm BIC} = 2.16$. (b) Q factor of the topological BIC deduced from the peaks in (a) as a function of d_2.

in Fig. 4(a) for the interface states between two semi-infinite PCs.

To show the spatial localization of the interface state between two PCs, we plot in Fig. 7(b) the square modulus of the electric field along the finite horizontal structure illustrated in Fig. 1(g) for the Tamm state labeled 1 at $\Omega = 0.58$ in Fig. 7(a). As predicted, the Tamm state is strongly localized at the interface between the two PCs and decreases in the bulk of these two systems.

In order to check the robustness of the topological BIC against structural perturbations in comparison with other interface modes of the system, we introduce a disorder by changing the lengths of the stubs and periods of two PCs, each one being made of $N = 5$ cells. We keep the cavity of length $\frac{d_1+d_2}{2}$ and the two surrounding stubs of lengths $d_1' = 1$ unperturbed and we introduce the disorder in the other lengths of the stubs and periods around this cavity. Figure 8(a) shows a zoom of the DOS spectra versus Ω and d_2 of the upper

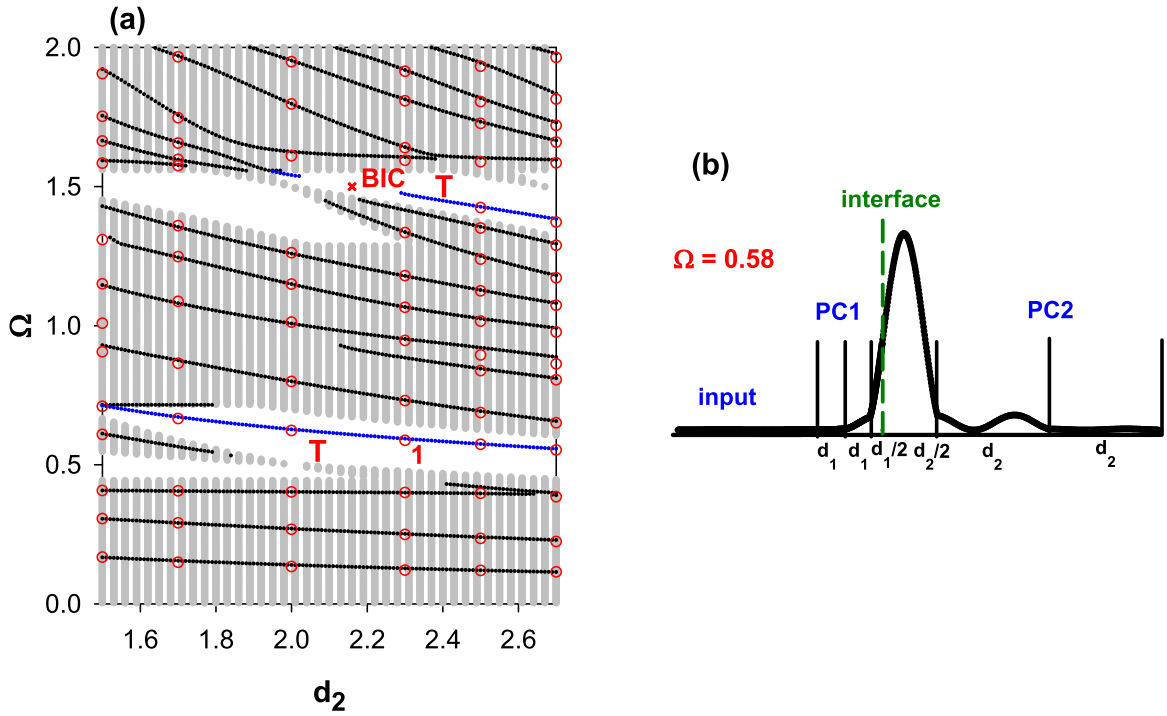

FIG. 7. (a) Reflection minima deduced from the reflection spectra inside the gaps (white areas) and bulk bands (gray areas) as a function of d_2 and Ω for $d_1 = 0.5$ m and $d_1' = d_2' = 1$ m. Open circles give the experimental measurements deduced from the minima of the reflection spectra for certain values of d_2. T refers to the topological interface branch and the cross indicates the position of the BIC. (b) Square modulus of the electric field along the two finite horizontal PCs illustrated in Fig. 1(g) for the Tamm state labeled 1 in (a) at $\Omega = 0.58$.

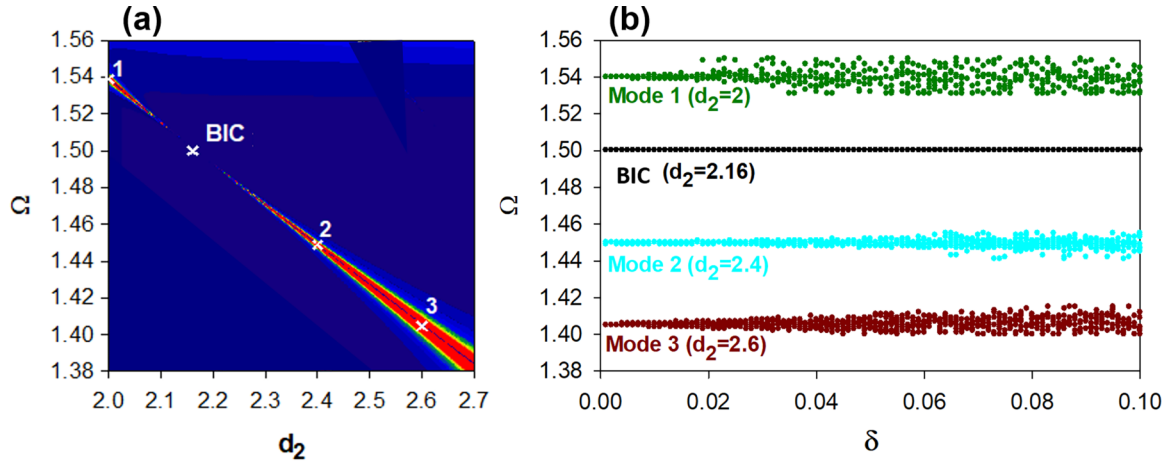

FIG. 8. (a) Zoom of DOS spectra (in color scale) in the upper common gap around $\Omega_{\mathrm{BIC}} = 1.5$ and $d_2^{\mathrm{BIC}} = 2.16$. (b) Evolution of the interface states marked by crosses in (a) for 10 realizations of disorder by varying the disorder strength δ for: BIC (blue curve), mode 1 (green curve), mode 2 (cyan curve), and mode 3 (brown curve).

interface branch. In order to compare the robustness of the BIC with three other modes labeled 1 to 3 near to the BIC [Fig. 8(a)], we numerically implement a disorder realization of strength δ ranging from zero (unperturbed system) to 0.1 (perturbed system). The lengths of the periods d_i are uniformly random in the interval $[d_i - \delta d_i, d_i + \delta d_i]$ $(i = 1, 2)$, and the lengths of the stubs $d_i' = 1$ are uniformly random in the interval $[d_i' - \delta d_i', d_i' + \delta d_i']$ $(i = 1, 2)$. For each strength of perturbation, 10 different disorder realizations were considered. Figure 8(b) gives a comparison of the effect of the disorder on the BIC (at $d_2^{\mathrm{BIC}} = 2.16$) and the three modes labeled 1 to 3 in Fig. 8(a). The results in Fig. 8(b) are obtained from the variation of the DOS in Fig. 8(a) which gives a signature of the BIC mode at $\Omega = 1.5$. As predicted, one can see that BIC is much more robust to the disorder strength δ in comparison with the other modes; this is due to the property of the BIC which is a decoupled mode from the rest of the system and depends only on the cavity of length $\frac{d_1+d_2}{2}$ surrounded by two stubs of lengths d_1' with vanishing electric field at their connection points. As δ increases, the BIC stays pinned at the same frequency $\Omega = 1.5$, while the other modes fluctuate. Also, one can notice that as d_2 goes away from $d_2^{\mathrm{BIC}} = 2.16$, the mode becomes more sensitive to the disorder strength.

To give an experimental evidence of the idea discussed in Fig. 3(f) about the existence of two topological interface states when two PCs are taken exactly at two successive flat bands, we give in Fig. 9 an example of two successive flat bands labeled 2 (at $d_1 = \frac{2}{3}$) and 3 (at $d_1 = \frac{4}{3}$) in Fig. 3(f) which fall at the same frequency $\Omega = 1.5$. Figures 9(a) and 9(b) represent the band structures for PC5 with $d_1 = \frac{2}{3}$ and PC6 with $d_1 = \frac{4}{3}$. The colors in the gaps and band edges have the same meaning as in Fig. 3. These two PCs exhibit two consecutive common gaps separated by a flat band at $\Omega = 1.5$ and the symmetries of their band edges are different. Therefore, if we combine these two PCs (PC5-PC6), one can predict two topological interface states in the two successive common gaps. However, there is no interface state in the lower common gap (around $\Omega = 0.6$) since the lower band edges of PC5 and PC6 are characterized by the same symmetries (or equivalently by the same sign of the reflection phase). This result is confirmed in the reflection amplitude and the corresponding delay time and DOS for a finite PC made of PC5-PC6 in Figs. 9(c) and 9(d). The common gaps between the two PCs are indicated by gray areas. Solid lines represent the theoretical results in presence of loss, while open circles give the experimental measurements. We can see that there is no interface state in the lower common gap of PC5-PC6 and two interface states appear in the two common gaps around $\Omega = 1.5$ [Fig. 9(c)]. These two modes appear also as well-defined peaks in the variation of the DOS (green dashed lines) in Fig. 9(d). In the presence of loss, these modes appear as negative delta peaks in the reflection delay time (blue lines and open circles).

Let us mention here that all these discussions about topological interface states and their behaviors in the different scattering parameters can be also obtained by considering a transmission configuration consisting of two finite PCs inserted between two semi-infinite waveguides [Fig. 1(h)]. The results of this configuration are given in the Supplemental Material SM4 [67].

D. Experimental results: Vertical structure

In this section, we propose another configuration to observe all the eigenmodes of two combined PCs and in particular the topological interface states. The structure consists in two finite PCs grafted vertically along a waveguide [Fig. 1(i)]. The advantage of the vertical structure lies in the possibility to deduce the eigenmodes of the isolated structure [Fig. 1(f)] with either $H = 0$ or $E = 0$ boundary condition at its bottom side. As it was demonstrated in Sec. II C, the eigenmodes of the two finite PCs with $E = 0$ boundary condition at the bottom side and $H = 0$ boundary condition at the top side of the structure can be obtained from the zeros of the transmission $t_v = 0$ [i.e., $\tau = 0$ in Eq. (20)]. Similarly, the eigenmodes of the two finite PCs with $H = 0$ boundary condition on both sides of the structure can be deduced from the zeros of the reflection coefficient $r_v = 0$ [i.e., $\rho = 0$ in Eq. (21)], or equivalently from the maxima of the transmission. Figure 10 illustrates the eigenmodes of the finite structure depicted in

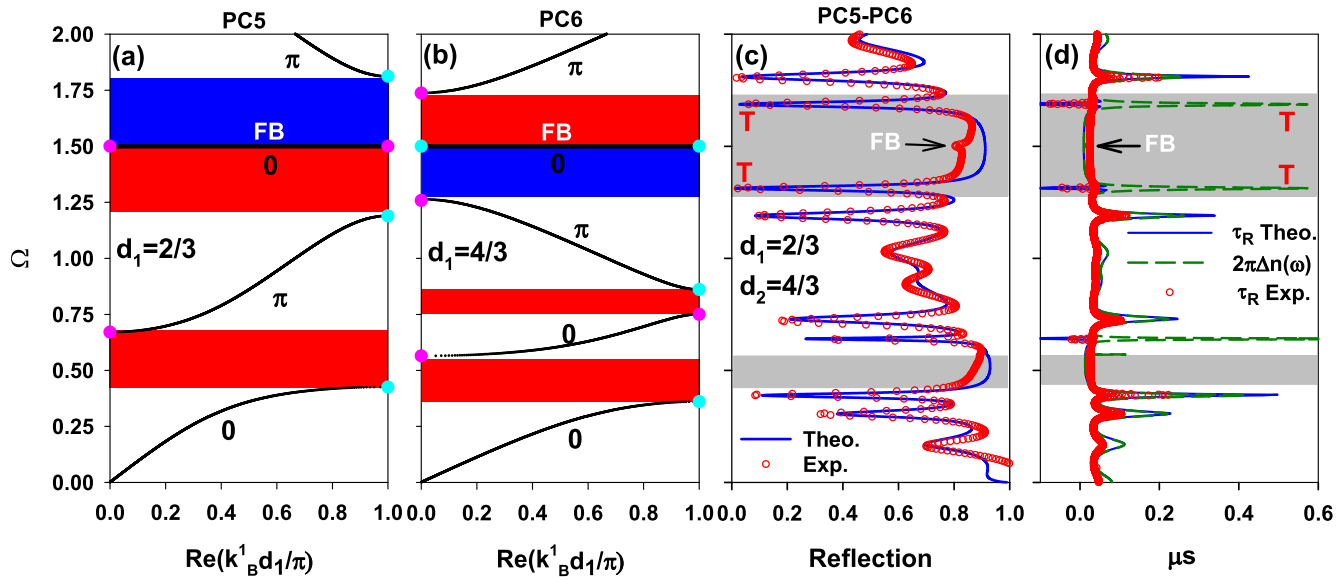

FIG. 9. (a), (b) Band-gap structures for PC5 with $d_1 = \frac{2}{3}$ and PC6 with $d_1 = \frac{4}{3}$ corresponding to flat bands 2 and 3 in Fig. 3(f), respectively. The Zak phases of each bulk band are labeled by 0 or π. The pink and cyan dots represent the symmetric and antisymmetric band-edge states, respectively. The gaps are colored in blue or red depending on whether the sign of the reflection phase is negative or positive. (c) Reflection amplitude for a finite PC made of PC5-PC6. Gray areas indicate common gaps between the two PCs. (d) The corresponding delay time in comparison with the variation of the DOS [$2\pi\,\Delta n(\omega)$]. Solid lines represent the theoretical results in presence of loss, while open circles give the experimental measurements. Green dashed curve in (d) gives the variation of the DOS.

Fig. 1(f) as a function of d_2 for $d_1 = 0.5$ and $d_1' = d_2' = 1$. The shaded areas show the common bulk bands of the infinite systems, while white areas represent the common gaps as a function of d_2. In Fig. 10(a), we report the eigenmodes (black curves) of two finite PCs, each one being composed of $N = 2$ stubs with $H = 0$ on both sides. These modes are obtained from the maxima of the transmission coefficient [i.e., $\rho = 0$ in Eq. (20)]. Within the common gaps (white areas), the green branches represent the topological interface states. Open circles give the experimental results which reproduce

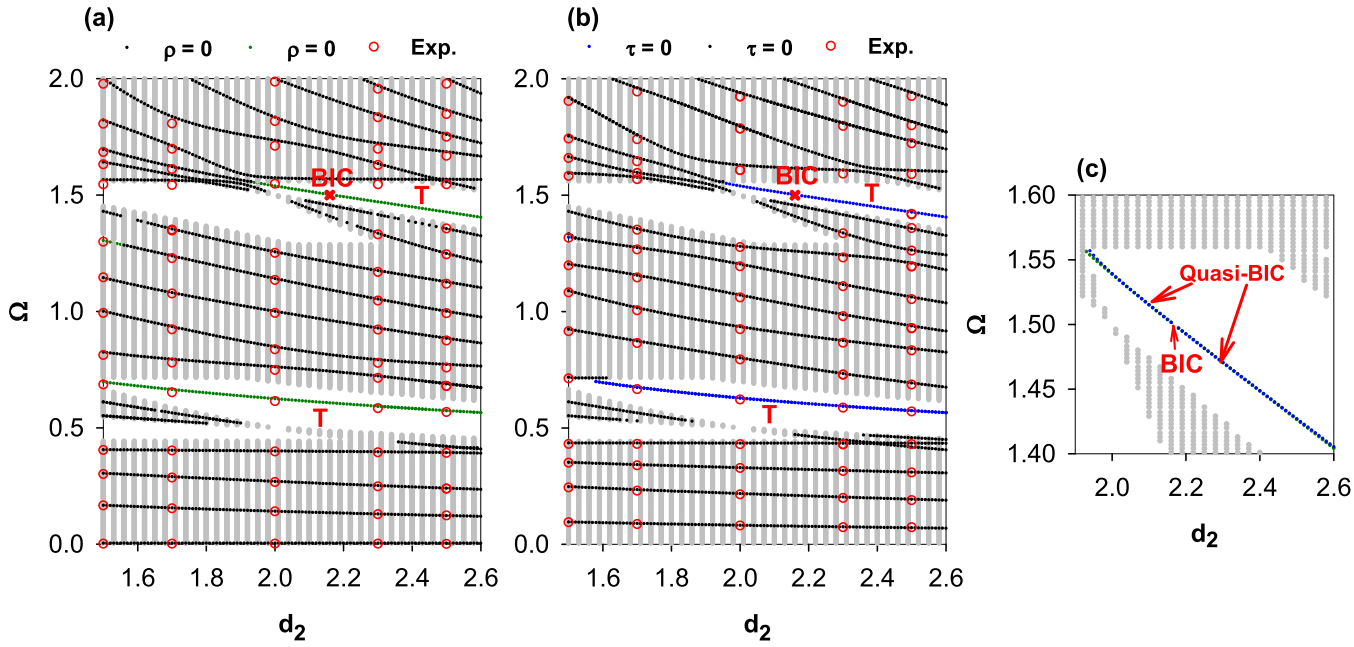

FIG. 10. (a) Eigenmodes of two finite PCs [Fig. 1(f)] with $H = 0$ boundary condition on their both sides as a function of d_2 and Ω for $d_1 = 0.5$ and $d_1' = d_2' = 1$. (b) Same as in (a) but for $E = 0$ boundary condition at the bottom side and $H = 0$ boundary condition at the top side of two finite PCs [Fig. 1(f)]. T refers to the topological interface branch and the cross indicates the position of the BIC. (c) Zoom of the interface branch in the upper common gap around BIC at $\Omega_{\rm BIC} = 1.5$ and $d_2^{\rm BIC} = 2.16$.

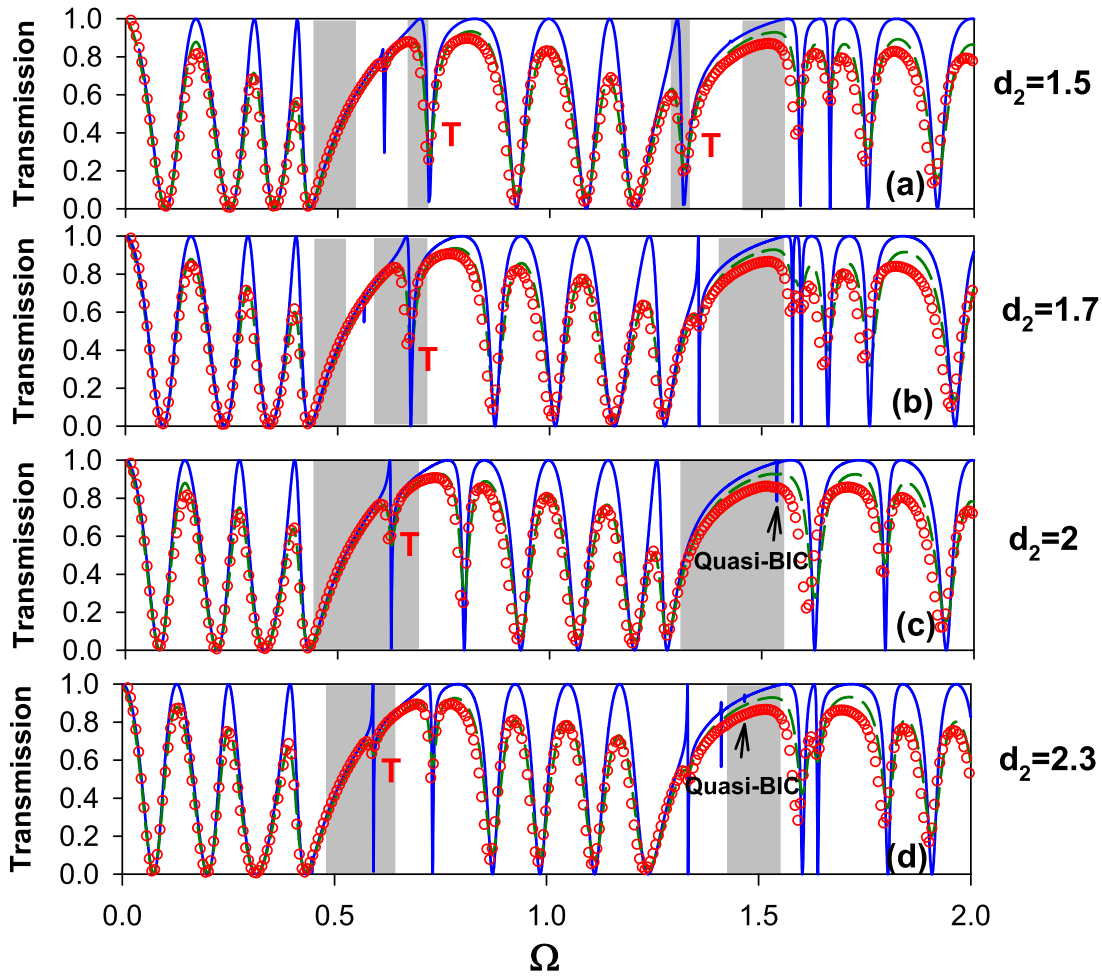

FIG. 11. (a)–(d) Transmission spectra as a function of Ω for $d_1 = 0.5$, $d_1' = d_2' = 1$ and some values of d_2 for the vertical configuration in Fig. 1(i) such that (a) $d_2 = 1.5$, (b) $d_2 = 1.7$, (c) $d_2 = 2$, and (d) $d_2 = 2.3$. Blue and green dashed curves represent the theoretical results without and with loss, respectively, while open circles show the experimental results. T refers to the topological interface state lying inside the common gaps (gray areas).

very well the theoretical results inside the bulk bands and within the lower common gap around $\Omega = 0.6$, while the modes inside the upper common gap around $\Omega = 1.5$ are not detected because this upper branch falls near to the BIC. The modes around the BIC become very narrow in the spectra (see below) which prevents their observation due to the loss in the system. These results corroborate those obtained previously in Fig. 7(a). Similarly, Fig. 10(b) shows the eigenmodes of the finite structure with $E = 0$ at the bottom side and $H = 0$ at the top side of the structure. These modes are obtained from the minima of the transmission coefficient [i.e., $\tau = 0$ Eq. (20)]. In general, the eigenmodes inside the bulk bands of both structures in Figs. 10(a) and 10(b) are different; however, the branches associated to the interface states inside the common gaps are very close, the small difference resulting from the finite sizes of the two PCs. This is shown in Fig. 10(c) where we plot both interface branches (green and blue) in the upper gap. We can see that these two branches are very close to each other as the interface modes weakly depend on the boundary conditions at the extremities of the structure and coincide exactly at the BIC for which $\tau = \rho = 0$, while around the BIC we have $\tau \simeq \rho \simeq 0$ and these modes can be qualified as quasi-BICs.

Figure 11 shows some examples of the transmission spectra for the vertical structure [Fig. 1(i)] for $d_1 = 0.5$, $d_1' = d_2' = 1$ and some values of d_2 such as $d_2 = 1.5$ [Fig. 11(a)], $d_2 = 1.7$ [Fig. 11(b)], $d_2 = 2$ [Fig. 11(c)], and $d_2 = 2.3$ [Fig. 11(d)]. The blue and green curves represent the theoretical results without and with loss, while open circles correspond to the experimental data. For $d_2 = 1.5$ [Fig. 11(a)] the interface mode appears in the second and third common gaps (gray areas). For $d_2 = 1.7$ [Fig. 11(b)], the interface state appears only in the second common gap around $\Omega = 0.7$. This interface state appears in the shape of a Fano resonance [74] (i.e., a maximum of the transmission in the vicinity of a minimum of the transmission). For $d_2 \geqslant 2$ [Figs. 11(c) and 11(d)] an interface state starts to appear also in the upper common gap as a quasi-BIC for the lossless system (blue curve). This interface state appears in the shape of a Fano resonance, its width decreases as d_2 increases until it becomes a BIC for $d_2^{\mathrm{BIC}} = 2.16$ and $\Omega_{\mathrm{BIC}} = 1.5$ and reappears again when d_2 deviates from the BIC position. In the experiments

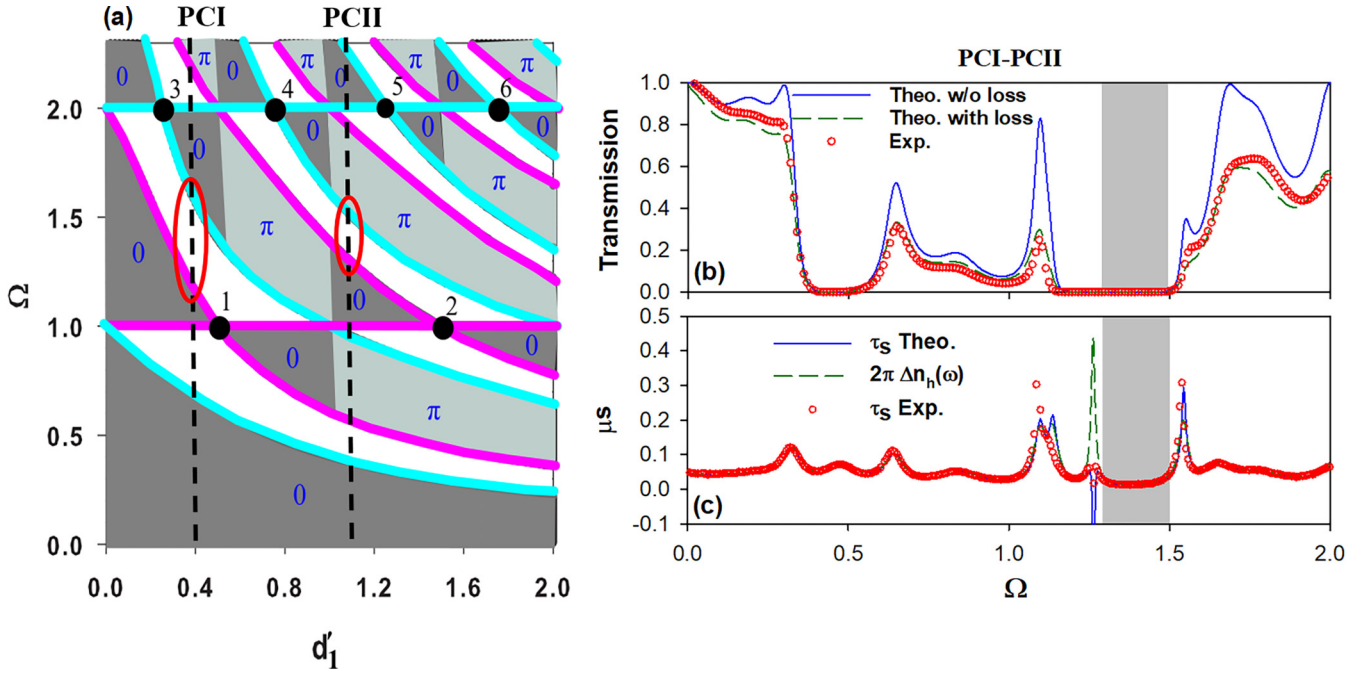

FIG. 12. (a) Band-gap structure as a function of the length of the stub d_1' and Ω for a fixed period at $d_1 = 1$. The black dots 1 to 6 indicate the flat bands where the bands close and reopen. Gray and dark cyan colors give the bands where the Zak phase is 0 or π, respectively. (b) Theoretical and experimental transmission coefficient for PCI-PCII in the case of the horizontal configuration in Fig. 1(h). The lengths of the stubs are chosen such that $d_1' = 0.4$ m, $d_2' = 1.1$ m, and fixed periods $d_1 = d_2 = 1$ m. Blue and green dashed curves represent the theoretical results without and with loss, respectively, while open circles show the experimental results. (c) Derivative of the phase of $\det(S_h)$ (noted τ_s) as a function of Ω (blue and red circles), and the variation of the DOS $[2\pi\,\Delta n_h(\omega)]$ (green dashed curves).

(open circles), the interface state in the upper common gap is not detected because of the losses in the cables that prevent the observation of a very-high-quality mode before considering the dissipation.

It is worth mentioning that the three configurations in Figs. 1(g)–1(i) support each other and show the same interface states in the different scattering parameters.

IV. EFFECT OF THE LENGTHS OF THE STUBS

In all the previous results, we have fixed the lengths of the stubs at $d_1' = d_2' = 1$ and discussed the existence of topological interface states as a function of the length of the periods d_1 and d_2. Here, we show the impossibility of existence of interface states as a function of the lengths of the stubs when both PCs have the same period. To this end, we display in Fig. 12(a) the band-gap structure of an infinite PC as a function of the length of the stubs d_1' and $\Omega = \frac{\omega d_1}{c\pi}\sqrt{\varepsilon}$ for a fixed period $d_1 = 1$ m. Black dots 1 to 6 indicate the position of the flat bands, i.e., the band-crossing points where the bands close and reopen. These points are given by

$$\frac{d_1'}{d_1} = \frac{2m_1'}{2m_2' + 1} \tag{37}$$

and the dimensionless frequency

$$\Omega = m_1'. \tag{38}$$

Points 1 to 6 in Fig. 12(a) correspond to the pairs $(m_1', m_2') = (1, 0), (1, 1), (2, 0), (2, 1), (2, 2)$, and $(2, 3)$, respectively. By varying d_1', one can obtain a common gap of two PCs chosen appropriately. The symmetries of the band-edge states are shown by pink and cyan colors for symmetric and antisymmetric states, respectively. From the symmetry argument, one can deduce the Zak phase of the bulk bands as a function of d_1'. The Zak phases of the bulk bands are indicated by gray and dark cyan colors for 0 and π, respectively. It can be noticed that all the common gaps are characterized by the same symmetry at their lower and upper band-edge states (i.e., both symmetric or both antisymmetric) whatever the value of d_1'. Therefore, it is impossible to get an interface state in any common gap of two PCs with different values of d_1' and the same periods $d_1 = d_2 = 1$. For example, if we consider two PCs with $d_1' = 0.4$ and $d_1' = 1.1$ [labeled PCI and PCII in Fig. 12(a)], one can obtain a large common gap of these two PCs around $\Omega = 1.3$ (indicated by large circles), however, this gap cannot support an interface state. To confirm this result, we plotted in Figs. 12(b) and 12(c) the theoretical and experimental transmission and DOS spectra for PCI-PCII in the case of the horizontal configuration in Fig. 1(h) (see the Supplemental Material SM4 [67]). As predicted, it can be seen clearly that there is no interface state within the common gap indicated by the gray area in Figs. 12(b) and 12(c).

Finally, it is worth mentioning that all the discussions about the existence of topological interface states and their

properties in the scattering parameters can be also obtained for Dirichlet boundary condition, i.e., vanishing of the electric field ($E = 0$) at the end of the stubs. These results are discussed in the Supplemental Material SM5 [67].

V. CONCLUSION

In several papers, the concept of topological Tamm states between two one-dimensional photonic crystals is discussed in the frame of the SSH model based on band inversion around a gap closure. In this work, we proposed a concept based on band inversion around a band closure (i.e., a flat band). This concept is demonstrated in a simple platform composed of periodic stubs with different lengths and periods. The advantage of such a mechanism lies in the existence of common gaps of hybridization type where the Tamm states are very well localized in comparison with the usual Bragg gaps. In particular, there are two interface states in such gaps when two PCs exhibit flat bands that fall at the same frequency in the middle of a large common gap with different band-edge symmetries. The existence of these interface states is proved both theoretically and experimentally through an analysis of the dispersion relations, Zak phases, densities of states, scattering matrix, and transmission and reflection coefficients for two connected PCs. Also, we have given the analytical expressions of the geometrical parameters and the frequency when the Tamm states transform to BICs. We have shown that these BICs are induced by the cavity between the two PCs and are protected from any perturbation or disorder on both sides of the cavity. Finally, we have shown the impossibility of existence of interface states between two PCs with similar periods and different stubs. The theoretical and experimental results are discussed for Neumann ($H = 0$) boundary conditions at the end of the stubs. The results for the case Dirichlet ($E = 0$) boundary conditions are postponed to the Supplemental Material SM5 [67]. All these results can be straightforwardly transposed to acoustic waves in slender tubes [65,75] and plasmonic metal-insulator-metal waveguides operating in the telecommunication domain [43,76].

[1] I. Tamm, Phys. Z. Sowjetunion **1**, 733 (1932).
[2] S. G. Davison and M. Steslicka, *Basic Theory of Surface States* (Clarendon Press, Oxford, 1992).
[3] M. Stęślicka, R. Kucharczyk, A. Akjouj, B. Djafari-Rouhani, L. Dobrzynski, and S. G. Davison, Surf. Sci. Rep. **47**, 93 (2002).
[4] P. Yeh, A. Yariv, and C. S. Hong, J. Opt. Soc. Am. **67**, 423 (1977).
[5] P. Yeh, *Optical Waves in Layered Media* (Wiley, New York, 1988).
[6] M. L. Bah, A. Akjouj, E. H. El Boudouti, B. Djafari-Rouhani, and L. Dobrzynski, J. Phys.: Condens. Matter **8**, 4171 (1996).
[7] A. P. Vinogradov, A. V. Dorofeenko, A. M. Merzlikin, and A. A. Lisyansky, Phys. Usp. **53**, 243 (2010).
[8] M. Kaliteevski, I. Iorsh, S. Brand, R. A. Abram, J. M. Chamberlain, A. V. Kavokin, and I. A. Shelykh, Phys. Rev. B **76**, 165415 (2007).
[9] M. Sasin, R. Seisyan, M. Kalitteevski, S. Brand, R. Abram, J. Chamberlain, A. Y. Egorov, A. Vasilev, V. Mikhrin, and A. Kavokin, Appl. Phys. Lett. **92**, 251112 (2008).
[10] F. Ramos-Mendieta and P. Halevi, J. Opt. Soc. Am. B **14**, 370 (1997).
[11] M. L. H. Lahlaouti, A. Akjouj, B. Djafari-Rouhani, L. Dobrzynski, M. Hammouchi, E. H. El Boudouti, A. Nougaoui, and B. Kharbouch, Phys. Rev. B **63**, 035312 (2001).
[12] F. Villa and J. A. Gaspar-Armenta, Opt. Commun. **223**, 109 (2003).
[13] P. Yeh, A. Yariv, F. Villa, and A. Y. Cho, Appl. Phys. Lett. **32**, 104 (1978).
[14] W. Ng, P. Yeh, P. C. Chen, and A. Yariv, Appl. Phys. Lett. **32**, 370 (1978).
[15] A. A. Bulgakov and V. R. Kovtun, Opt. Spektrosk. **56**, 769 (1984) [Opt. Spectrosc. **56**, 471 (1984)].
[16] R. D. Meade, K. D. Brommer, A. M. Rappe, and J. D. Joannopoulos, Phys. Rev. B **44**, 10961 (1991).
[17] S. Ya. Vetrov and A. V. Shabanov, Zh. Eksp. Teor. Fiz. **101**, 1340 (1992) [Sov. Phys. JETP **74**, 719 (1992)].
[18] W. M. Robertson and M. S. May, Appl. Phys. Lett. **74**, 1800 (1999).
[19] S. Shukla, S. Prasad, and V. Singh, Phys. Plasmas **22**, 022122 (2015).
[20] O. El Abouti, E. H. El Boudouti, Y. El Hassouani, A. Noual, and B. Djafari-Rouhani, Phys. Plasmas **23**, 082115 (2016).
[21] D. Smirnova, P. Buslaev, I. Iorsh, I. V. Shadrivov, P. A. Belov, and Y. S. Kivshar, Phys. Rev. B **89**, 245414 (2014).
[22] A. Madani and S. Roshan Entezar, Super. Microst. **75**, 692 (2014).
[23] A. Namdar, I. V. Shadrivov, and Y. S. Kivshar, Appl. Phys. Lett. **89**, 114104 (2006).
[24] A. Namdar, Opt. Commun. **278**, 194 (2007).
[25] Y. Xiang, P. Wang, W. Cai, C. F. Ying, X. Zhang, and J. Xu, J. Opt. Soc. Am. B **31**, 2769 (2014).
[26] L. Niu, Y. Xiang, W. Cai, X. Zhao, N. Zhang, J. Qi, X. Zhang, and J. Xu, J. Opt. Soc. Am. B **35**, 1368 (2018).
[27] Y. El Hassouani, H. Aynaou, E. H. El Boudouti, B. Djafari-Rouhani, A. Akjouj, and V. R. Velasco, Phys. Rev. B **74**, 035314 (2006).
[28] E. H. El Boudouti, Y. El Hassouani, B. Djafari-Rouhani, and H. Aynaou, Phys. Rev. E **76**, 026607 (2007).
[29] J. Guo, Y. Sun, Y. Zhang, H. Li, H. Jiang, and H. Chen, Phys. Rev. E **78**, 026607 (2008).
[30] A. Kavokin, I. Shelykh, and G. Malpuech, Appl. Phys. Lett. **87**, 261105 (2005).
[31] A. V. Kavokin, I. A. Shelykh, and G. Malpuech, Phys. Rev. B **72**, 233102 (2005).
[32] T. Goto, A. V. Dorofeenko, A. M. Merzlikin, A. V. Baryshev, A. P. Vinogradov, M. Inoue, A. A. Lisyansky, and A. B. Granovsky, Phys. Rev. Lett. **101**, 113902 (2008).
[33] E. Descrovi, F. Frascella, B. Sciacca, F. Geobaldo, L. Dominici, and F. Michelotti, Appl. Phys. Lett. **91**, 241109 (2007).

[34] T. Fort, R. Kanok, P. Hlubina, P. Pokorny, and J. Sobota, Photonics **9**, 561 (2022).

[35] M. A. Kaliteevski, A. A. Lazarenko, N. D. Il'inskaya, Yu. M. Zadiranov, M. E. Sasin, D. Zaitsev, V. A. Mazlin, P. N. Brunkov, S. I. Pavlov, and A. Yu. Egorov, Plasmonics **10**, 281 (2015).

[36] H. Lu, T. Zhu, J. Zhang, H. C. Liu, K. S. Shen, Y. Zheng, S. Q. Dong, S. Q. Xia, C. Dong, X. K. Li, W. Y. Luo, X. L. Sun, X. Z. Zhang, and C. H. Xue, Opt. Express **29**, 17736 (2021).

[37] C. Symonds, G. Lheureux, J. P. Hugonin, J. J. Greffet, J. Laverdant, G. Brucoli, A. Lemaître, P. Senellart, and J. Bellessa, Nano Lett. **13**, 3179 (2013).

[38] M. Xiao, Z. Q. Zhang, and C. T. Chan, Phys. Rev. X **4**, 021017 (2014).

[39] M. Atala, M. Aidelsburger, J. T. Barreiro, D. Abanin, T. Kitagawa, E. Demler, and I. Bloch, Nat. Phys. **9**, 795 (2013).

[40] Q. Wang, M. Xiao, H. Liu, S. Zhu, and C. T. Chan, Phys. Rev. B **93**, 041415(R) (2016).

[41] W. S. Gao, M. Xiao, C. T. Chan, and W. Y. Tam, Opt. Lett. **40**, 5259 (2015).

[42] A. Juneau-Fecteau and L. G. Fréchette, Opt. Mater. Express **8**, 2774 (2018).

[43] Y. Rezzouk, M. Amrani, S. Khattou, and B. Djafari-Rouhani, J. Opt. Soc. Am. B **39**, 600 (2022).

[44] Z. Chen, P. Han, C. W. Leung, Y. Wang, M. Hu, and Y. Chen, Opt. Express **20**, 21618 (2012).

[45] S. Elshahat, Z. E. A. Mohamed, M. Almokhtar, and C. Lu, J. Opt. **24**, 035004 (2022).

[46] L. Wang, W. Cai, M. Bie, X. Zhang, and J. Xu, Opt. Express **26**, 28963 (2018).

[47] J. C. G. Henriques, T. G. Rappoport, Y. V. Bludov, M. I. Vasilevskiy, and N. M. R. Peres, Phys. Rev. A **101**, 043811 (2020).

[48] O. Ortiz, P. Priya, A. Rodriguez, A. Lemaitre, M. Esmann, and N. D. Lanzillotti-Kimura, Optica **8**, 598 (2021).

[49] M. Esmann, F. R. Lamberti, P. Senellart, I. Favero, O. Krebs, L. Lanco, C. Gomez Carbonell, A. Lemaître, and N. D. Lanzillotti-Kimura, Phys. Rev. B **97**, 155422 (2018).

[50] G. Cáceres-Aravena, B. Real, D. Guzmán-Silva, A. Amo, L. E. F. Foa Torres, and R. A. Vicencio, Phys. Rev. Res. **4**, 013185 (2022).

[51] W. Zhu, Y.-q. Ding, J. Ren, Y. Sun, Y. Li, H. Jiang, and H. Chen, Phys. Rev. B **97**, 195307 (2018).

[52] M. Seki, M. Saigusa, M. Nemoto, K. Kusama, T. Tobita, M. Kuriyama, and K. Uehara, Phys. Rev. Lett. **62**, 1989 (1989).

[53] D. Xiao, M.-C. Chang, and Q. Niu, Rev. Mod. Phys. **82**, 1959 (2010).

[54] J. Cayssol and J. N. Fuchs, J. Phys. Mater. **4**, 034007 (2021).

[55] W. P. Su, J. R. Schrieffer, and A. J. Heeger, Phys. Rev. Lett. **42**, 1698 (1979).

[56] C. W. Hsu, B. Zhen, A. D. Stone, J. D. Joannopoulos, and M. Soljacic, Nat. Rev. Mater. **1**, 16048 (2016).

[57] E. N. Bulgakov, and D. N. Maksimov, Phys. Rev. Lett. **118**, 267401 (2017).

[58] A. Cerjan, M. Jürgensen, W. A. Benalcazar, S. Mukherjee, and M. C. Rechtsman, Phys. Rev. Lett. **125**, 213901 (2020).

[59] B. Zhen, C. W. Hsu, L. Lu, A. D. Stone, and M. Soljacic, Phys. Rev. Lett. **113**, 257401 (2014).

[60] Q. Song, M. Zhao, L. Liu, J. Chai, G. He, H. Xiang, D. Han, and J. Zi, Phys. Rev. A **100**, 023810 (2019).

[61] Y. X. Xiao, G. Ma, Z. Q. Zhang, and C. T. Chan, Phys. Rev. Lett. **118**, 166803 (2017).

[62] J. O. Vasseur, A. Akjouj, L. Dobrzynski, B. Djafari-Rouhani and E. H. El Boudouti, Surf. Sci. Rep. **54**, 1 (2004).

[63] L. Dobrzynski, A. Akjouj, E. H. El Boudouti, G. Lévêque, H. Al-Wahsh, Y. Pennec, C. Ghouila-Houri, A. Talbi, B. Djafari-Rouhani, and Y. Jin, *Photonics* (Elsevier, Amsterdam, 2020), Chap. 11.

[64] S. Khattou, Y. Rezzouk, M. Amrani, M. El Ghafiani, E. H. El Boudouti, A. Talbi, and B. Djafari-Rouhani, Crystals **12**, 1685 (2022).

[65] W. M. Robertson, C. Vazquez, J. Lopez, A. LaVerde, and R. J. Giuntini, AIP Adv. **12**, 045018 (2022).

[66] S. Khattou, Y. Rezzouk, M. Amrani, M. El Ghafiani, E. H. El Boudouti, and B. Djafari-Rouhani (unpublished).

[67] See Supplemental Material at http://link.aps.org/supplemental/10.1103/PhysRevB.107.125405 for the details of the analytical calculations of the elements a_i and b_i (SM1), the details of the experimental setup (SM2), the effect of loss on the reflection amplitude and reflection delay time (SM3), the results of the horizontal structure between two semi-infinite waveguides (SM4), and the results of DBC ($E = 0$) at the end of the stubs (SM5).

[68] J. Friedel, London, Edinburgh, Dublin Philos. Mag. J. Sci. **43**, 153 (1952).

[69] S. Khattou, M. Amrani, A. Mouadili, El H. El Boudouti, A. Talbi, A. Akjouj, and B. Djafari-Rouhani, Phys. Rev. B **102**, 165310 (2020).

[70] B. Djafari-Rouhani, E. H. El Boudouti, A. Akjouj, L. Dobrzynski, J. O. Vasseur, A. Mir, N. Fettouhi, and J. Zemmouri, Vacuum **63**, 177 (2001).

[71] M. M. Tirkey and N. Gupta, Int. J. Microw. Wireless Technol. **11**, 151 (2019).

[72] C. Yan, M. Pu, J. Luo, Y. Huang, X. Li, X. Ma, and X. Luo, Opt. Laser Technol. **101**, 499 (2018).

[73] C. Poli, M. Bellec, U. Kuhl, F. Mortessagne, and H. Schomerus, Nat. Commun. **6**, 6710 (2015).

[74] U. Fano, Phys. Rev. **124**, 1866 (1961).

[75] S. Khattou, M. Amrani, A. Mouadili, and B. Djafari-Rouhani, Mater. Today: Proc. **45**, 7394 (2021).

[76] S. Khattou, M. Amrani, A. Mouadili, E. H. El Boudouti, A. Talbi, A. Akjouj, and B. Djafari-Rouhani, J. Appl. Phys. **131**, 153102 (2022).